

Protoplanetary Disks and Their Evolution

JONATHAN P. WILLIAMS AND LUCAS A. CIEZA

Institute for Astronomy, University of Hawaii, Honolulu, HI 96822, USA

Key Words pre-main-sequence stars, circumstellar matter, accretion, planet formation

Abstract Flattened, rotating disks of cool dust and gas extending for tens to hundreds of AU are found around almost all low mass stars shortly after their birth. These disks generally persist for several Myr, during which time some material accretes onto the star, some is lost through outflows and photoevaporation, and some condenses into centimeter- and larger-sized bodies or planetesimals. Through observations mainly at infrared through millimeter wavelengths, we can determine how common disks are at different ages, measure basic properties including mass, size, structure, and composition, and follow their varied evolutionary pathways. In this way, we see the first steps toward exoplanet formation and learn about the origins of the Solar System. This review addresses observations of the outer parts, beyond 1 AU, of protoplanetary disks with a focus on recent infrared and (sub-)millimeter results and an eye to the promise of new facilities in the immediate future.

CONTENTS

INTRODUCTION	2
CLASSIFICATION OF YOUNG STELLAR OBJECTS	3
DISK FORMATION	5
<i>Section summary</i>	7
PROPERTIES OF PROTOPLANETARY DISKS	7
<i>Mass</i>	8
<i>Radius</i>	9
<i>Structure</i>	11
<i>Composition</i>	14
<i>Dependence on stellar mass</i>	18
<i>Section summary</i>	18
DISK LIFETIMES	19
<i>Near-infrared results: the inner disk</i>	19
<i>Spitzer results: the planet-forming regions of the disk</i>	20
<i>Dissipation timescale</i>	22
<i>Dependence on stellar mass</i>	22
<i>Gas dispersal</i>	23
<i>Environmental influences</i>	23
<i>Section summary</i>	26
DISK EVOLUTION	27
<i>Viscous transport</i>	27

<i>Photoevaporation by radiation from the central star</i>	27
<i>Grain growth and dust settling</i>	29
<i>Typical evolution and diversity of evolutionary paths</i>	32
<i>Section summary</i>	34
TRANSITION DISKS	34
<i>SED diversity and interpretation</i>	35
<i>Incidence</i>	36
<i>Physical properties</i>	37
<i>Resolved observations</i>	38
<i>Section summary</i>	39
SUMMARY POINTS	39
FUTURE ISSUES	40
Acknowledgements	42

1 INTRODUCTION

Circumstellar disks are an inevitable consequence of angular momentum conservation during the formation of a star through gravitational collapse. Initially disks rapidly funnel material onto the star but, as the surrounding molecular core is used up or otherwise disperses, the accretion rate decreases and a small amount of material persists. That these disks can be considered protoplanetary is apparent not only through the geometry of the Solar System but also the high detection rate of exoplanets.

Because disks exhibit a range of temperatures – hot near the star, cooler farther away – they radiate strongly at a range of wavelengths from microns to millimeters. They can therefore be observed with infrared and radio telescopes, and the mapping of wavelength to radius allows detailed models of their structure to be determined purely from unresolved photometry. Furthermore, their longevity, relative to the natal core, allows their properties to be studied in relation to the optically visible protostar.

Internal friction, or viscosity, within the disk drives continued accretion onto the star. To preserve angular momentum, some material is lost through outflows and the disk may gradually spread out with time. Its structure may also be strongly affected by photoevaporation, both from the central star and external stars, and by the agglomeration of dust grains well beyond the typical sizes found in the interstellar medium including, ultimately, into planetesimals large enough to gravitationally perturb the disk. The various evolutionary pathways lead to inner holes and gaps that reveal themselves through a relative decrement in flux over a narrow range of wavelengths and which may also be imaged directly at sufficiently high resolution.

The Infrared Astronomical Satellite (*IRAS*) opened up the infrared sky and allowed the first statistical studies of disk occurrence to be made (Strom et al. 1989). Shortly thereafter the first sensitive detectors at millimeter wavelengths showed that many disks contained large dust grains (Weintraub, Sandell & Duncan 1989) with enough material to form planetary systems on the scale of our own (Beckwith et al. 1990). Interferometry at these long wavelengths provided the ability to resolve the rotation in the disks (Sargent & Beckwith 1987), but unequivocal evidence for their flattened morphology actually came in the optical,

with the Hubble Space Telescope (*Hubble*), through exquisite images of disk shadows against a bright nebular background (O’dell & Wen 1994). The pace of discoveries has accelerated in the past decade due to increases in sensitivity, resolution, and wavelength coverage. The Infrared Space Observatory (*ISO*) and, in particular, the Spitzer Space Telescope (*Spitzer*) have greatly expanded the known disk inventory in terms of central stellar mass, age, environment, and evolutionary state. Interferometry has expanded to longer baselines and shorter wavelengths, including into the sub-millimeter regime with the Submillimeter Array (*SMA*), providing the ability to map fainter structures in greater detail. The potential to address fundamental questions in protoplanetary disk studies provided significant motivation for the development of major new facilities including the Herschel Space Observatory (*Herschel*) and Atacama Large Millimeter/submillimeter Array (*ALMA*).

The rather short history of protoplanetary disk research may be followed in the regular Protostars and Planets series (Black & Matthews 1985, Gehrels 1978, Levy & Lunine 1993, Mannings, Boss & Russell 2000, Reipurth, Jewitt & Keil 2007). There are also several related reviews that have been recently written for this series including the inner disk (Dullemond & Monnier 2010), debris disks (Wyatt 2008), and dynamical processes (Armitage 2010).

This review focuses on the properties and evolution of the outer parts of protoplanetary disks around low mass stars as determined principally from observations at mid-infrared to millimeter wavelengths. After briefly describing the classification of young stellar objects in §2, we begin by discussing the formation of disks in §3 and their basic properties when the central star first becomes optically revealed in §4. The second half concerns itself with the temporal properties of disks. We discuss their lifetimes in §5, the evidence for, and processes by which, disks evolve in §6, and the properties of disks transitioning into their end state in §7. Each section ends with a short summary of the key points and these, in turn, are distilled into an overall summary in §8. There are many promising avenues for future exploration that new and planned facilities can address, and we list those that we deem most exciting in §9.

2 CLASSIFICATION OF YOUNG STELLAR OBJECTS

The process of star and planet formation begins with the collapse of a molecular core. The mass is initially all in the core but it is processed through an accretion disk inward onto the protostar and outward through an outflow. Ultimately the core is dispersed and the remaining mass is concentrated in the star. There is enough terminology associated with this process to form its own “diskionary” (Evans et al. 2009a) and many observational ways to characterize the progression. The most direct, that of measuring the mass in each component, is hard and more practical means are generally used, principally measuring disk accretion signatures in the optical or the distribution of warm circumstellar material in the infrared.

The infrared based classification dates back to Lada & Wilking (1984) who showed that Young Stellar Objects (YSO) in Ophiuchus formed 3 distinct groups based on whether the emitted energy was rising in the mid-infrared, declining but with a notable excess over the blackbody stellar photosphere, or with negligible infrared excess. This was formalized into 3 classes, I-II-III respectively, by Lada

(1987) based on the slope of the spectral energy distribution (SED) between about 2 and 25 μm ,

$$\alpha_{\text{IR}} = \frac{d \log \nu F_\nu}{d \log \nu} = \frac{d \log \lambda F_\lambda}{d \log \lambda}. \quad (1)$$

Greene et al. (1994) subsequently introduced an additional refinement of “flat-spectrum sources”, intermediate between Class I and II YSOs. The class sequence was shown to fit naturally into the theoretical framework of a rotating, collapsing core by Adams, Lada & Shu (1987). As the ability to detect faint millimeter emission improved, the categorization was extended to an earlier, Class 0, phase by André, Ward-Thompson & Barsony (1993) and the decrease in mass of the circumstellar envelope (material participating in the star/disk formation) along the sequence was verified (André & Montmerle 1994).

A parallel accretion-based classification exists for the later optically visible phases: classical and weak-lined T Tauri stars. These correspond closely (though not exactly) to Class II and III YSOs respectively. Classical T Tauri stars (CTTS) have strong H α and UV emission whereas weak-lined T Tauri stars (WTTS) show no or only very low indications of accretion. Historically the dividing line between the two was a uniform H α equivalent width of 10 Å but this has been refined to a stellar mass dependent limit to account for the lower continuum level in low mass stars (Barrado y Navascués & Martín 2003, White & Basri 2003). The census of Class III sources or WTTS is generally incomplete in optical and infrared catalogs because they lack strong accretion signatures and infrared excesses. Their youth is generally only betrayed through their location in the Hertzsprung-Russell diagram above the main sequence or by X-ray activity (Feigelson & Montmerle 1999).

It is also important to note that the SED classification does not give a unique description of the amount and distribution of circumstellar material. In particular, YSOs with edge-on disks are highly extincted and can be mis-interpreted as more embedded, hence, less evolved, objects. For example, a Class II YSO viewed at high inclination has a similar SED to a typical Class I YSO and an edge-on Class I YSO can have characteristics of a Class 0 YSO (Robitaille et al. 2006). These ambiguities highlight the necessity to distinguish between the physical “stage” of YSO evolution for comparison to theory and its observed SED. Resolved images, ideally at multiple wavelengths, are required to fully characterize the evolutionary state of any individual YSO. Table 1 summarizes the definitions for each class, where the numerical boundaries for α_{IR} follow Greene et al. (1994), including corresponding physical properties (evolutionary stage) and other observational characteristics.

A disk forms very early on and grows rapidly during the Class 0 collapse phase (see §3). On average, the embedded phases through Class I lasts for about ~ 0.5 Myr (Evans et al. 2009b). The surrounding envelope and strong protostellar outflows can hinder measurements of disk properties at these early times. The properties of the disks as their central stars first become optically visible, i.e. Class II YSOs, are discussed in §4. The median disk lifetime after the embedded phase is 2–3 Myr but the manner and the rate at which any individual star-disk system evolves vary greatly. These issues are discussed extensively in §§5, 6.

Large *Spitzer* surveys have mapped about 90% of all the star-forming regions within 500 pc of the Sun (Evans et al. 2009b, and references therein) and spectra have been obtained for over 2000 YSOs therein (e.g., Furlan et al. 2009, Kessler-Silacci et al. 2007, Oliveira et al. 2010). The precision and wavelength

coverage of these observations show the tremendous diversity of disk SEDs and the inadequacy of a single parameter, α_{IR} , to characterize the full range, especially as disks dissipate and open up central holes. These so-called transition disks are the subject of §7.

3 DISK FORMATION

The initial collapse of a molecular cloud core is onto a point source but a disk quickly forms as more distant material with higher angular momentum falls inward. The disk extends out to the centrifugal radius, which is expected to grow rapidly with time, $R(t) \propto \Omega^2 t^3$, where Ω is the angular rotation rate of the core (Terebey, Shu & Cassen 1984). Disks should evolve rapidly, therefore, and their final size and mass depends sensitively on the infall time (t^3) and the core properties (Ω^2). Basu (1998) notes that magnetized collapsing cores may not be in rigid rotation and that the radius may grow only linearly with time. In any case, given the wide range of core rotation rates (Goodman et al. 1993) and likely variation in infall duration, we should not be surprised by an inherent and large diversity in initial disk sizes and masses.

The role of magnetic fields in core collapse and disk formation is uncertain. Polarization measurements show magnetic field lines concentrating at the center of collapsing cloud cores in a pinched, “hour glass” configuration (Girart, Rao & Marrone 2006) yet Zeeman observations show that the magnetic field strength is generally insufficient to support cores against their own gravity (Crutcher, Hakobian & Troland 2009). We expect some field lines to be dragged down to disk scales for the magneto-rotational instability, the most likely mechanism for disk viscosity at late times, to exist. Singledish sub-millimeter measurements of polarization in disks (Tamura et al. 1999) have not been confirmed with interferometry, however, thus challenging theoretical understanding (Hughes et al. 2009b).

Numerical models of both magnetic and non-magnetic collapsing molecular cores show disks form rapidly, within $\sim 10^4$ yr (Hueso & Guillot 2005; Yorke, Bodenheimer & Laughlin 1993). Temperatures are very high in these early stages due to gravitational infall. As the core material is used up or otherwise dispersed, the disk cools down and its mass decreases as it accretes onto the star.

Core collapse onto a disk opens up an approximately spherical cavity in the surrounding envelope of radius $R(t)$ that has been inferred from the presence of excess mid-infrared emission above that expected from a more extincted centrally peaked core (Enoch et al. 2009, Jørgensen et al. 2005b). Although there are many observations of inward motions on core-size scales (e.g., Di Francesco et al. 2001), the direct detection of gas flow onto a disk has yet to be convincingly demonstrated. Chandler et al. (2005) find SO line absorption against the disk continuum in the IRAS 16293-2422B YSO but the spectral profile is approximately symmetric about the source velocity and cannot be clearly identified as pure infall. Watson et al. (2007) detect many mid-infrared lines of H_2O toward NGC1333-IRAS4B, which they model as arising from a dense, warm, and compact region. They attribute this to shocked gas from an envelope onto a disk surface. However, Jørgensen & van Dishoeck (2010) mapped the 1.5 mm $3_{1,3} - 2_{2,0}$ transition of H_2^{18}O from the ground and find the water emission is quiescent and follows the disk rotation.

Imaging embedded disks requires long wavelengths to see through the en-

velopes and arcsecond or higher resolution to match the disk sizes. Millimeter interferometers meet these requirements and also filter out extended structures so that the emission from the compact disk dominates on long baselines, $\gtrsim 50\text{k}\lambda$ (e.g., Brown et al. 2000, Jørgensen et al. 2005a, Keene & Masson 1990, Looney, Mundy & Welch 2000). A 1.1 mm continuum survey of 20 embedded YSOs by Jørgensen et al. (2009) shows that the disk flux is an average of four times higher in the embedded Class 0 phase than in Class I sources but, after allowing for higher temperatures due to greater accretion heating, the inferred disk masses show no significant dependence on evolutionary state. Masses in both Class 0 and I sources range from $\sim 0.02 - 0.1 M_{\odot}$ with a median $0.04 M_{\odot}$. This is quantitatively similar to the results from 2.7 mm observations of 6 sources by Looney, Mundy & Welch (2003).

The lack of dependence of disk mass on evolutionary state from Class 0 to Class I is contrary to theoretical expectations of steady disk growth as outlined above, whether the core is rigidly or differentially rotating. Rather, it indicates that disks form quickly and that the flow of material from the envelope, which declines in mass by almost an order of magnitude between these two classes (Young et al. 2003), is rapidly transported through the disk.

A likely cause of the rapid transport at these early stages is disk instability. Laughlin & Bodenheimer (1994) first suggested that disks would be gravitationally unstable during the early formation stages due to the relatively high mass fraction in the disk versus that accreted onto the protostar. The instabilities would lead to sporadic bursts of high accretion (Zhu et al. 2009) and prevent the disk mass from growing faster than the star (Vorobyov & Basu 2010). Many protostars have been observed to undergo short-lived bursts of activity due to high accretion and these events are named after the first such identified case, FU Orionis (Herbig 1977). Hartmann & Kenyon (1996) estimate that a typical low mass star may have an average of about 10 such outbursts during its formation.

Additional supporting observational evidence for “punctuated evolution” at these early stages is found in measurements of mass infall rates through the different components and the protostellar luminosity distribution. Eisner et al. (2005) find envelope infall rates are more than an order of magnitude higher than disk accretion rates in Class I YSOs suggesting that mass builds up in the disk until a burst event occurs. It has long been known that Class I YSOs are, on average, about an order of magnitude less luminous than expected for the steady release of gravitational energy as the envelope falls onto the protostar over the lifetime of the embedded phase (Kenyon et al. 1990). Based on the statistics from the cores-to-disks *Spitzer* survey of 5 large, nearby molecular clouds, Evans et al. (2009b) concludes that, on average, a star gains half of its final mass in only $\sim 7\%$ of the ~ 0.5 Myr Class 0 plus I lifetime. These statistics can be matched by models of episodic mass accretion from self-gravitating disks (Dunham et al. 2010).

Some words of caution are necessary in the interpretation of the interferometric data, however. The analyses of the continuum visibilities are based on rather sparse sampling of the Fourier plane and are subject to confusion with small scale structure in the envelope (Chiang et al. 2008). A more secure identification of an embedded disk requires spectral line observations showing rotation. The emission from the core and any protostellar outflow may still present significant confusion, although this is somewhat mitigated by observing species such as HCN and HCO^+ that only emit substantially in gas that is warmer and denser than the outer parts

of the envelope. Recent work demonstrates the possibilities in this area with indications of Keplerian velocity profiles in moderately young, Class I sources (Brinch et al. 2007, Jørgensen et al. 2009, Lommen et al. 2008). More sensitive observations of optically thin isotopologues are required to discern disk kinematics from the core background in the younger, more embedded Class 0 phase. Such observations also have the potential to measure the central protostellar mass and track its growth against the evolution of the envelope and disk.

3.1 Section summary

- Circumstellar disks form almost immediately after a molecular core collapses. Their existence can be inferred through both SED modeling and interferometry.
- Disk masses do not appear to increase with time during core collapse implying a rapid transport onto the star.
- The low average luminosity of YSOs and the accretion bursts of FU Orionis objects suggest that young disks are (gravitationally) unstable.

4 PROPERTIES OF PROTOPLANETARY DISKS

The deeply embedded Class 0 and I phases of star formation only last for a small fraction of a disk lifetime, typically ~ 0.5 Myr compared to several Myr. By the end of the Class I phase the envelope has completely dispersed and the star formation process is effectively over. The disk now contains only a few percent of the central stellar mass and can be considered truly protoplanetary, not protostellar. Although there may be a small amount of accretion of material from the molecular cloud, the major elements governing the evolution of the disk at this stage are accretion onto the star, photo-evaporation from local or external radiation sources, agglomeration into larger bodies, and dynamical interactions with stellar or substellar companions.

Unless the disk is edge-on to our line of sight, the extinction to the central protostar is small and its spectral type can be determined through optical or near-infrared spectroscopy in most cases. The properties of the disks at this stage marks the baseline for studies of their evolution and for core accretion models of giant planet formation. In this section, we discuss the basic properties of the outer regions of protoplanetary disks around Class II YSO.

As a fiducial comparison, we use the Minimum Mass Solar Nebula (MMSN), the lowest mass primordial disk that formed the Solar System inferred from scaling planetary compositions to cosmic abundances at each orbital radius (Kusaka, Nakano & Hayashi 1970; Weidenschilling 1977). Because of the uncertainty in the composition of the giant planets, Weidenschilling (1977) quotes a range for the MMSN of $0.01 - 0.07 M_{\odot}$. Here, we use the minimum of this range, $0.01 M_{\odot} \approx 10 M_{\text{Jup}}$, as an absolute lower mass for the solar nebula out to the 30 AU orbit of Neptune. Extrasolar planetary systems have been found around 10% of Sun-like stars in the solar neighborhood, and many planets detected to date are considerably more massive than Jupiter (Johnson 2009). The minimum mass disk required for their formation is proportionally higher.

The extrapolated surface density profile, which is an observable for resolved disks, has an approximate power law form, $\Sigma \propto r^{-3/2}$, although more sophisti-

cated fits based on viscous disk evolution and planet migration models can be made (Davis 2005, Desch 2007).

The properties of the outer parts ($\gtrsim 1$ AU) of protoplanetary disks are mainly inferred from observations at mid-infrared through millimeter wavelengths although optical and near-infrared scattered light or silhouette observations can provide important information on disk radii and dust grain properties (Pinte et al. 2008, Throop et al. 2001).

4.1 Mass

Disk masses are best determined from (sub-)millimeter wavelength observations of dust. The continuum emission is optically thin except in the innermost regions where column densities are very high. The optical depth is the integral of the dust opacity, κ_ν , times the density, ρ , along the line of sight, $\tau_\nu = \int \rho \kappa_\nu ds = \kappa_\nu \Sigma$, where Σ is the projected surface density. A commonly used prescription for the dust opacity in disks at millimeter wavelengths is

$$\kappa_\nu = 0.1 \left(\frac{\nu}{10^{12} \text{ Hz}} \right)^\beta \text{ cm}^2 \text{ g}^{-1} \quad (2)$$

(Beckwith et al. 1990). Both the absolute value and power law index, β , are related to the size distribution and composition of the dust grains (Ossenkopf & Henning 1994, Pollack et al. 1994). The normalization above also implicitly includes a gas-to-dust ratio of 100, and ρ and Σ refer to the total (gas plus dust) density.

For disks, $\beta \approx 1$ so $\kappa(1 \text{ mm}) = 0.03 \text{ cm}^2 \text{ g}^{-1}$ which implies $\tau(1 \text{ mm}) = 1$ at a surface density of $\Sigma \approx 30 \text{ g cm}^{-2}$, corresponding to about 10 AU in the MMSN (Davis 2005) and an angular scale of 0.07 in the nearby Taurus star-forming region. Protoplanetary disks are generally much larger than this and most of the resolved emission is indeed optically thin. However, the inner 10 AU likely constitutes a substantial fraction of the planet-forming region of a disk. Not only high resolution but also wavelengths longer than 1 mm are required to peer into this zone at the early phases of disk evolution.

For the general question of disk mass measurements on scales much larger than 10 AU, we can consider the emission to be optically thin and therefore directly relate the observed flux, F_ν , to the mass,

$$M(\text{gas} + \text{dust}) = \frac{F_\nu d^2}{\kappa_\nu B_\nu(T)}, \quad (3)$$

where d is the distance to the source. This shows an additional advantage of millimeter wavelengths in that the Planck function is close to the Rayleigh-Jeans regime, $B_\nu \approx 2\nu^2 kT/c^2$, and the emission is only linearly, rather than exponentially, dependent on the dust temperature.

The first large millimeter wavelength surveys to measure disk masses were carried out at 1.3 mm using a single element bolometer by Beckwith et al. (1990). in Taurus-Auriga and André & Montmerle (1994) in Ophiuchus. Both regions are predominantly forming low mass stars, $M_* < 1 M_\odot$ with spectral types K-M. Using bolometer arrays, which provide better sky subtraction capability, hence lower noise levels and the ability to detect fainter targets, Andrews & Williams (2005, 2007a) augmented these surveys in size and expanded the wavelength coverage into the sub-millimeter regime with observations from 350 μm to 850 μm .

The results of this work show that the median mass of Class II YSO disks is $5 M_{\text{Jup}}$ and the median ratio of disk to stellar mass is 0.9%. Figure 1 shows the mass distributions are rather flat by logarithmic mass interval with a steep decline beyond $\sim 50 M_{\text{Jup}}$. The explicit labeling of the gas-to-dust ratio in this figure mimics an earlier review by Beckwith & Sargent (1996) and serves to illustrate the large extrapolation necessary to derive total disk masses and constrain models of giant planet formation. This figure also includes the disk census by Mann & Williams (2010) in the more distant but massive star forming Orion region where photoevaporation is important (see §5.6.2).

By modeling the infrared-millimeter SED, Andrews & Williams (2005) showed that the simple mass derivation in equation 3 is indeed reasonably accurate with a characteristic temperature, $T = 20$ K. This temperature is consistent with CO observations (Qi et al. 2004) and theoretical expectations (Chiang & Goldreich 1997). Andrews & Williams (2005) also show that for a 100 AU disk with the mass and surface density profile of the MMSN, about one third of the emission by mass is optically thick at $850 \mu\text{m}$.

An additional major uncertainty is the hidden mass in large grains. Dust grows to much larger sizes in protoplanetary disks than in the interstellar medium and these “pebbles” or “snowballs” can hold considerable mass in a small solid angle with negligible effect on the SED. As a rule of thumb, observations at a wavelength λ only constrain the properties of dust grains out to a maximum size $a_{\text{max}} \sim 3\lambda$ (Draine 2006). Only a few disks have only been detected beyond millimeter wavelengths, and thus we know little about the general occurrence and distribution of centimeter and larger sized particles in disks. For a grain size distribution $n(a) \propto a^{-3.5}$ (Mathis, Rumpl & Nordsieck 1977), the total mass scales as $a_{\text{max}}^{1/2}$ and substantial mass may be undetected. Detailed modeling by D’Alessio, Calvet & Hartmann (2001) shows that the opacity prescription in equation 2 is valid for $a_{\text{max}} \sim 0.3 - 3$ mm but is about a factor of 20 smaller for $a_{\text{max}} = 1$ m implying correspondingly higher masses. The observational evidence for grain growth from sub-micron to millimeter sizes and beyond is discussed in §6.3.

The uncertainties in disk mass measurements are large but fortuitously tend to cancel each other out. We overestimate by assuming an interstellar gas-to-dust ratio and underestimate by ignoring large bodies. There are a couple of indications that disk masses as derived from equations 2 and 3 are significantly low, however, which would imply that grain growth is the dominant effect. First, protoplanetary disk masses derived from (sub-)millimeter photometry are systematically lower than those estimated from accretion rates integrated over protostellar ages (Andrews & Williams 2007a, Hartmann et al. 1998). Second, there are not enough massive disks in nearby star-forming regions to match the statistics on the incidence of extrasolar giant planets (Greaves & Rice 2010).

4.2 Radius

Disk sizes are hard to measure because the outer parts are cool and emit weakly. They are still efficient absorbers, however, and images of disk silhouettes in Orion against the optically bright HII region background provide a simple and direct size determination. Vicente & Alves (2005) measure radii ranging from 50 to 194 AU for 22 Orion “proplyds” where the disk shadow can be clearly seen in *Hubble* optical images and an additional two outliers with radii of 338 and 621 AU. The latter

object, cataloged as proplyd 114-426, is almost $3''$ in angular extent, resolved in both radial and vertical dimensions, and provides perhaps the most famous disk image obtained to date (McCaughrean et al. 1998, McCaughrean & O’dell 1996). Most of the Orion proplyds are apparent only through the photoevaporative flows from their surfaces, however, and Vicente & Alves (2005) estimate radii for 125 such objects from the size of the ionization front. Although there is substantial uncertainty associated in this indirect determination, they infer a median radius ~ 75 AU. They further note that the sample of *Hubble* proplyds accounts for only half the stars with known infrared excesses and suggest that over three quarters of the full sample of Orion disks have radii less than 75 AU.

Imaging disks at millimeter wavelengths requires interferometry on account of their small angular scales in nearby star-forming regions. Dutrey et al. (1996) carried out the first large interferometric survey and resolved many Taurus disks with typical angular sizes of $1-2''$. A curious problem arose in that the size of the gas disk, as observed in rotational lines of CO, was found to significantly exceed the size of the continuum image (Isella et al. 2007; Piétu, Guilloteau & Dutrey 2005). The differences could not be reconciled for a sharply truncated power law surface density profile (i.e., $\Sigma \propto R^{-p}$ for $R \leq R_{out}$, $\Sigma = 0$ for $R > R_{out}$) without introducing an arbitrary change in either the dust-to-gas ratio or dust opacity at the radius of the continuum disk. Similarly, McCaughrean & O’dell (1996) found that pure power laws or sharp edges do not match the intensity profiles of Orion proplyd silhouettes and showed that an exponential decay at the outer boundary was required. Indeed physical models of viscous accretion disks (e.g., Hartmann et al. 1998, Lynden-Bell & Pringle 1974), predict an exponentially tapered profile of the form,

$$\Sigma(R) = (2 - \gamma) \frac{M_d}{2\pi R_c^2} \left(\frac{R}{R_c} \right)^{-\gamma} \exp \left[- \left(\frac{R}{R_c} \right)^{2-\gamma} \right], \quad (4)$$

where M_d is the disk mass, R_c is a characteristic radius, and γ specifies the radial dependence of the disk viscosity, $\nu \propto R^\gamma$. Kitamura et al. (2002) first modeled millimeter wavelength disk images with this profile, but their data were unable to differentiate between this and sharply truncated power law fits. With higher resolution observations, Hughes et al. (2008) showed that this prescription can naturally account for the apparent size discrepancy in millimeter imaging as the the optically thick CO line can be detected further out along the tapered edge than the optically thin dust continuum.

R_c is a characteristic radius that delineates where the surface density profile begins to steepen significantly from a power law. As the disk does not have a sharp edge, a physical disk size must be specified in terms of an intensity threshold. A rough estimate of R_c may be obtained by noting that about 2/3 of the total disk mass (approximately flux) lies within it. More precisely, Hughes et al. (2008) determine $R_c = 30 - 200$ AU for four disks by fitting the profile in equation 4 to the continuum data. They compare with sharply truncated power law fits and find $R_{out} \approx 2R_c$. The tapered disks extend well beyond R_{out} , however, with midplane densities $n(\text{H}_2) > 10^5 \text{ cm}^{-3}$ for $R \lesssim 800$ AU.

By simultaneously fitting $850 \mu\text{m}$ interferometric visibilities and infrared-millimeter SEDs, Andrews et al. (2009, 2010b) determine a wide range $R_c = 14 - 198$ AU for 16 disks in Ophiuchus. Their sample is sufficiently large that they are able to identify a correlation with disk mass, $M_d \propto R_c^{1.6 \pm 0.3}$, which is likely to be a

signature of disk formation physics rather than an evolutionary sequence. They do not find any correlation with the central star properties.

Isella, Carpenter & Sargent (2009) use the same density prescription to fit a sample of 11 disks mostly in Taurus-Auriga. They use a slightly different radial normalization that converts to a similar range, $R_c \simeq 30 - 230$ AU, and also shows that the older disks tend to be larger. In addition, Schaefer et al. (2009) compile radii for 16 disks around low mass stars in Taurus-Auriga based on sharply truncated power law fits to CO observations. Because of the different fitting technique, their values, $R_{out} \sim 100 - 1100$ AU, are not directly comparable with the above R_c measures, but they similarly illustrate the large range of disk sizes and independence on stellar type.

The specific angular momenta of protoplanetary disks, $j = J/M$, lies in the range $\log_{10} j [\text{cm}^2 \text{s}^{-1}] = 19.4 - 20.9$ (Andrews et al. 2010b; Isella, Carpenter & Sargent 2009). This is comparable to the giant planets in the Solar System, $\log_{10} j = 20.0 - 20.4$, but significantly lower than the observed values in molecular cores, $\log_{10} j = 20.8 - 22.6$ (Goodman et al. 1993). Either the angular momentum in a core is not efficiently transferred to the disk, or its value is overestimated due to the inherent smoothing of turbulent fluctuations in radial velocity observations (Dib et al. 2010).

4.3 Structure

The average radial, vertical, and velocity profiles of relatively bright and large disks can be determined through resolved observations and careful modeling of spectral energy distributions.

4.3.1 SURFACE DENSITY A resolved image of a disk at millimeter wavelengths provides not only a measure of its total mass and radius but also the distribution of mass, or surface density. Until recently this was characterized as a pure power law, $\Sigma \propto R^{-p}$, with values of p generally in the range $0 - 1$ (Andrews & Williams 2007b, Kitamura et al. 2002, Lay, Carlstrom & Hills 1997, Mundy et al. 1996, Wilner et al. 2000).

The exponential tapered fits of the form in equation 4 approximate a power law, $\Sigma \propto R^{-\gamma}$ for $R \ll R_c$, but the fitted values of $R_c \simeq 30 - 200$ AU correspond to $\lesssim 1''$ in all but the closest disks and γ is actually determined largely from the steepness of the exponential taper. The Hughes et al. (2008) comparison of pure power law versus exponentially truncated power law fits shows similar indices but with slightly steeper pure power law fits due to the soft edge, $\langle p \rangle = 1.2$, $\langle \gamma \rangle = 0.9$ for four disks.

From larger samples, Andrews et al. (2009, 2010b) find a tight range consistent with all having the same value $\langle \gamma \rangle = 0.9$. Using a different modeling technique, however, Isella, Carpenter & Sargent (2009) find a very wide range $\gamma = -0.8$ to 0.8 with mean $\langle \gamma \rangle = 0.1$ in their data. Negative values of γ correspond to decreasing surface densities for $R < R_c$ which may be an important signature of disk evolution (see §6) but these were also found in the smaller disks with $R_c < 100$ AU which are barely resolved and thus the hardest to characterize.

In general, all results agree that young protoplanetary disks have flatter central density profiles than the canonical power law $p = 1.5$ MMSN (Weidenschilling 1977). There is even more uncertainty in the density profile of the MMSN than its mass, however, and an exponential tapered power law fit by Davis (2005) has $\gamma = 0.5$. The more relevant comparison is of absolute values in the planet-forming

zone. Andrews et al. (2009, 2010b) infer surface densities, $\Sigma \approx 10 - 100 \text{ g cm}^{-2}$ at 20 AU, in their sample of Ophiuchus disks that are in good agreement with the MMSN (Figure 2).

Whereas the disk-to-star mass ratio may be very high during the initial stages of formation (§3), the Toomre Q parameter, $Q(R) = c\Omega/\pi G\Sigma$ where c is the sound speed and Ω the orbital angular velocity (Toomre 1964), is generally much greater than unity for these Class II YSO disks implying that they are gravitationally stable at all radii (Andrews et al. 2010b; Isella, Carpenter & Sargent 2009). The one possible exception is DG Tau, a young protostar with by far the most massive disk in the two surveys.

The inferred surface densities are increasingly uncertain closer to the star due to the limited resolution of the observations, $\gtrsim 20 \text{ AU}$, and also because the emission is becoming optically thick. As the discrepancy between Andrews et al. (2009, 2010b) and Isella, Carpenter & Sargent (2009) shows, different data and fits extrapolate to very different surface densities at the 5 – 10 AU orbital radii of Jupiter and Saturn. This is not only a critical region for understanding planet formation but also for disk structure. The density is so high here that the mid-plane is shielded from radiation and cosmic rays. Unless radioactive elements are sufficiently abundant (Turner & Drake 2009), the ionization fraction may be so low that matter is decoupled from the magnetic field and avoids the magneto-rotational instability (see §6.1). Current observations cannot address these issues, and they will remain a challenge until the combined requirements of high sensitivity and high resolution at long wavelengths are met (Wilner 2004). Note, however, that the uncertainty in the surface density is outweighed by the Keplerian increase in rotation rate and Class II YSO disks are gravitationally stable in their inner regions.

4.3.2 SCALE HEIGHT Protoplanetary disks are flared with a vertical scale height that increases with radius. Kenyon & Hartmann (1987) first suggested the possibility of flaring based on the large far-infrared excesses detected by *IRAS* that could not be explained by a spatially flat disk. Direct evidence for flared disks can be found in the beautiful *Hubble* images of Taurus disk silhouettes against the scattered light of the central star (Burrows et al. 1996, Padgett et al. 1999, Stapelfeldt et al. 1998) and in Orion against the nebular background (Smith et al. 2005).

Characterizing the disk scale height is essential for modeling the thermal, ionization and chemical structure of disks and, thence, for interpreting atomic and molecular line observations. It is also important for understanding disk evolution as the outer parts, with their low densities and large scale heights, are particularly susceptible to photoevaporative losses.

For an azimuthally symmetric disk in hydrostatic equilibrium, the density is a function of both radius, R , and vertical height, Z ,

$$\rho(R, Z) = \frac{\Sigma(R)}{\sqrt{2\pi}H} \exp\left(-\frac{Z^2}{2H^2}\right), \quad (5)$$

where $\Sigma(R)$ is defined in equation 4, and $H(R)$ is the scale height which depends on the competition between disk thermal pressure and the vertical component of stellar gravity. The disk temperature, in turn, depends on the amount of stellar radiation impacting the disk and therefore on its geometry. Chiang & Goldreich (1997) provide an elegant analytic solution to these coupled equations by ap-

proximating the radiative transfer with a hot surface layer that absorbs and reprocesses the starlight, which then heats a flared interior. They find an approximate power law dependence, $H \propto R^h$, with $h \approx 1.3 - 1.5$. D'Alessio et al. (1998) and Dullemond, van Zadelhoff & Natta (2002) iterate numerical solutions to the vertical disk structure and find similar results.

Observed disk SEDs have less mid-infrared emission than expected for this degree of flaring due to settling of dust grains toward the midplane (Chiang et al. 2001, D'Alessio et al. 1999). This flattening of the dust disk relative to the gas occurs very early in the evolution of a disk and is discussed further in §6.

4.3.3 VELOCITY Disk masses at the Class II stage and beyond are a small fraction of the central stellar mass. Their motions are therefore expected to be Keplerian. Velocity profiles have been measured for only a handful of disks. The difficulty lies in finding disks that are sufficiently young and therefore bright enough to image in a spectral line, generally a millimeter wavelength rotational line of CO or isotopologue, yet not contaminated by emission from the residual envelope or neighboring cloud.

Koerner, Sargent & Beckwith (1993) resolved the $^{13}\text{CO } J = 2 - 1$ line in the relatively large GM Aur disk and found the velocity profile was consistent with being Keplerian. Similarly, Dutrey, Guilloteau & Simon (1994) imaged the large circumbinary disk around GG Tau in $^{13}\text{CO } J = 1 - 0$ and used a Keplerian velocity profile to determine a total stellar mass of $1.2 M_{\odot}$. With improvements in instrumentation, leading to higher frequency and higher resolution observations, more studies followed shortly thereafter (e.g., Duvert et al. 1998; Mannings, Koerner & Sargent 1997).

Guilloteau & Dutrey (1998) modeled the CO $J = 1 - 0$ channel maps (images at different velocities) of DM Tau to show that a Keplerian velocity profile was not only consistent but was the best fit. This was further exploited in the survey by Simon, Dutrey & Guilloteau (2000) who determined dynamical masses for 9 systems and tested models of protostellar evolution. Schaefer et al. (2009) extended this work to later spectral types. As discussed in §3, Lommen and Brinch have used the same technique to derive protostellar masses at even earlier times in Class 0 and I YSOs. Spectral line observations also determine disk inclinations to our line of sight with high accuracy (e.g., Qi et al. 2004), which is necessary for detailed modeling and characterization of other disk properties.

Many of the aforementioned studies also note that the line emission is well fit by only rotational plus thermal broadening. High spectral resolution observations of the TW Hydra and HD163296 disks by Hughes et al. (2010) show that the turbulent component is subsonic, $\leq 10\%$ and 40% , of the sound speed respectively at the ~ 100 AU scales of their observations. Such a low level of turbulent stirring provides ideal conditions for grain settling and growth, planetesimal congregation, and protoplanetary accretion. Their data also show near-perfect Keplerian rotational profiles confirming that disk self-gravity does not appear to be significant in these objects (Figure 3).

4.3.4 DEPARTURES FROM AZIMUTHAL SYMMETRY The discussion in this section has so far considered only the radial or vertical variation of disk properties on account of the dominant gravity of the central star. Azimuthal variations are of great interest, however, because they would signpost an additional influence, potentially disk self-gravity or proto-planets.

Disks are tiny compared to the distances between stars even in dense clusters

and disruptive encounters are highly unlikely. For typical relative motions of 1 km s^{-1} , the stellar density must be greater than $\sim 10^6 \text{ stars pc}^{-3}$ for an encounter within 1000 AU of a disk within 1 Myr. Almost all disks that have been studied in detail are nearby and are either isolated or in low mass star-forming regions where the stellar densities are orders of magnitude lower than this. Consequently, the likelihood that any azimuthal distortions in a young disk are due to an encounter with a nearby star is very low.

The surface density measurements described in §4.3.1 and Keplerian velocity profiles in §4.3.3 show that disk self-gravity is negligible by the time of the Class II phase. As discussed in §3, however, younger disks in formation probably have much higher disk-to-star mass ratios. The disk around the partially embedded Herbig Ae star AB Aur may be an example of an unstable disk. Optical and near-infrared coronagraphic imaging by Grady et al. (1999) and Fukagawa et al. (2004) show spiral features in scattered light. Lower resolution millimeter interferometry confirms the larger scale asymmetries in the system (Corder, Eisner & Sargent 2005) and deviations from Keplerian rotation that may indicate streaming motions along the arms or an unseen companion (Lin et al. 2006; Piétu, Guilloteau & Dutrey 2005).

The gravitational effect of planets on debris disks has been diagnosed in Fomalhaut (Chiang et al. 2009), postulated in β Pic (Mouillet et al. 1997), and suspected in others (Wyatt 2008, and references therein). Younger disks are further away than these systems and, the intriguing case of AB Aur notwithstanding, the resolution is not yet sufficient to search for such effects, although this is an exciting prospect for the future (Narayanan et al. 2006, Wolf & D’Angelo 2005).

4.4 Composition

As with the interstellar medium, the circumstellar medium is composed of dust and gas. There is substantial processing of both components, however, as a disk forms and evolves.

4.4.1 DUST Dust dominates the opacity of protoplanetary disks and is the raw material for planetesimals. In the diffuse interstellar medium, dust is mainly composed of silicates with sizes $r \lesssim 0.1 \mu\text{m}$ with an admixture of graphite grains and polycyclic aromatic hydrocarbons (Draine 2003). During the passage through cold dark clouds to protoplanetary disks, molecules freeze out from the gas phase onto dust grain surfaces producing icy mantles (Bergin & Tafalla 2007) and the grains collisionally agglomerate (Blum & Wurm 2008).

Silicates are readily identified through broad spectral bands at 10 and $18 \mu\text{m}$ (Henning 2010). Polycyclic aromatic hydrocarbons also have several mid-infrared features in this wavelength range (Tielens 2008). About 2000 protoplanetary disks were observed with the Spitzer Infrared Spectrometer (IRS) providing a wealth of information on the composition, size distribution, and evolution of the dust. We defer discussion to §6.3 and note here only that the dust in disks has been significantly processed via thermal annealing and agglomeration to have a much higher crystallinity fraction and larger sizes relative to the interstellar medium.

4.4.2 GAS Gas amounts to 99% of the total mass of the interstellar medium and the same is true, at least initially, for disks. Its detection, however, presents a tougher observational challenge than the minority dust component because it

emits only at specific wavelengths and therefore requires high resolution spectroscopy. Moreover, at wavelengths where the dust emission is optically thick, a line can only be seen if its excitation temperature differs from that of the dust.

Disk accretion, which can be measured through recombination line emission or excess hot continuum emission, provides unambiguous evidence for the presence of gas. However, the precise amount or physical conditions of the gas in the disk cannot be determined from these diagnostics (Hartmann 2009).

At the typical high densities and low temperatures of the bulk of a protoplanetary disk, the primary gaseous species is H_2 . Fluorescent electronic transitions of H_2 in the UV arise from hot gas very close to the protostar (Herczeg et al. 2006). Near-infrared ro-vibrational lines also probe the inner disk, $\lesssim 1$ AU. Because the focus of this review is on the outer disk, we discuss mid-infrared observations of H_2 only and refer the reader to Najita et al. (2007) for details on the inner disk gas component.

As a symmetric molecule, H_2 has no electric dipole moment and only magnetic quadrupole transitions are permitted, i.e. $\Delta J = \pm 2$. These lines lie in the mid-infrared, with energies characteristic of the temperatures at several AU in a disk, a potentially very interesting regime for understanding giant planet formation. Bitner et al. (2007) detected and spectrally resolved 3 lines (H_2 S(1), S(2), S(4) corresponding to $J = 3 - 1, 4 - 2, 6 - 4$ respectively) in AB Aur. The linewidths locate the emitting region to 18 AU in radius but the rotational diagram indicates a temperature of 670 K, which is much hotter than the dust temperature at this radius. They infer that the gas is decoupled from the dust and excited by either protostellar UV or X-rays, or shocks from the infalling envelope (see also Bitner et al. 2008). Similarly, Martin-Zaïdi et al. (2007) detect the H_2 S(1) line in another intermediate mass Herbig Ae star, HD97048, and show that the high line-to-continuum ratio requires either an enhanced gas-to-dust ratio or an additional gas heating mechanism such as X-rays or shocks.

In both cases, the inferred gas mass is very small. For AB Aur, where the multiple lines allow the level populations to be determined, $M_{\text{H}_2} = 0.5 M_{\oplus} \simeq 0.1\%$ of the total disk mass. Effectively, only the top of the disk atmosphere is measured due to the high optical depth of the dust at these wavelengths. Based on the Chiang & Goldreich (1997) two-layer model, Carmona et al. (2008) calculate that mid-infrared H_2 detections require gas temperatures twice as high as the dust and a gas-to-dust ratio greater than 1000. This is possible through dust settling to the midplane but the low detection rates suggest that such extreme conditions are rare (Lahuis et al. 2007, Martin-Zaïdi et al. 2010).

Trace amounts, $M_{\text{HI}} \sim 1 M_{\oplus}$, of atomic hydrogen should also be present due to photodissociation of H_2 (Kamp, Freudling & Chengalur 2007). Although beyond the sensitivity of current instruments, it will be possible to detect the 21 cm line in many disks with the Square Kilometer Array (Kamp et al. 2008).

Fortunately, there are many other currently observable species present in disks from ionized and atomic at the disk surface to molecular deeper within. An interesting case is the optical line of [O I] at 6300 Å, which has been detected in the surface of strongly flared Herbig Ae/Be disks out to ~ 100 AU (Acke, van den Ancker & Dullemond 2005). It originates from the photodissociation of OH which results in excited neutral atomic oxygen.

Spitzer spectroscopy has provided many new results. [Ne II] is one of the strongest lines and has an origin in YSO jets (Güdel et al. 2010). For sources without jets, the [Ne II] line is much weaker and traces hot gas on the disk

surface, possibly from a photoevaporate flow (Pascucci & Sterzik 2009). Rotational lines from the organic molecules, C_2H_2 , HCN, and CO_2 , have also been detected by IRS, in absorption through a nearly-edge on disk by Lahuis et al. (2006), and in emission by Carr & Najita (2008). Assuming local thermodynamic equilibrium, both studies find molecular excitation temperatures in the range of 300 – 700 K, implying a location in the inner 3 – 6 AU of the disks. Their production is due to a rich gas phase chemistry sustained by the sublimation of icy grain mantles in a warm molecular region above the disk midplane, and is strongly dependent on the stellar radiation field. Pascucci et al. (2009) find a deficit of HCN in disks around very low mass stars and brown dwarfs, which they attribute to a reduced photodissociation rate of N_2 . Pontoppidan et al. (2010) find almost no molecular emission toward 25 Herbig Ae/Be stars (the exception being one CO_2 line). They suggest either photodissociation, lower gas-to-dust ratios, or masking by the strong continuum as the cause.

The bulk of the lines in the Carr & Najita (2008) IRS spectrum of AA Tau are rotational lines of OH and H_2O . These are important coolants and also of great astrobiological interest. Their derived high abundances require vertical and potentially radial transport of ices from the inner, cooler regions of the disk. Salyk et al. (2008) found similar results toward an additional two disks, and the large survey by Pontoppidan et al. (2010) shows that these lines are common in T Tauri disks. The complex origin of the gas-phase water and its implications for understanding disk structure and evolution have been recently discussed by Meijerink et al. (2009) and Ciesla & Cuzzi (2006).

There are also many detectable molecular lines in the (sub-)millimeter wavelength regime. Observations of low energy rotational transitions, which can be excited even at the low temperatures and densities of the outer disk, provide the best constraints on the total gas mass in a disk. CO lines are the strongest on account of its high abundance and large dipole moment. The dominant source of opacity in this case is not the dust but the lines themselves. Interferometric CO images therefore show the radial gas temperature gradient, $T \propto r^{-q}$, with values of $q \simeq 0.4 - 0.7$ for both T Tauri and Herbig Ae/Be stars (Guilloteau & Dutrey 1998, Piétu, Dutrey & Guilloteau 2007), which is in agreement with the dust temperature derived from SED modeling (Andrews & Williams 2005). Multi-transition observations trace different $\tau = 1$ surfaces providing information on the vertical temperature structure. Qi et al. (2006) show that the strong CO 6–5 emission of the TW Hydra disk requires a hot surface layer with a gas-dust temperature difference of up to 30 K that can be explained by X-ray heating. Observations of the rarer isotopologues, ^{13}CO and C^{18}O , probe deeper into the disk and show cooler midplane temperatures, ~ 13 K, and an order-of magnitude depletion of CO relative to the interstellar medium (Dartois, Dutrey & Guilloteau 2003). This is due to CO condensation onto dust grains at a temperature of about 20 K (Sandford & Allamandola 1993). Similarly high depletions have been found in other T Tauri disks (e.g., Öberg et al. 2010, Qi et al. 2004). The situation is quite different for disks around the more luminous Herbig AeBe stars where the dust is warmer than the CO condensation temperature throughout. Within the uncertainties of CO isotopologue abundance and dust opacity, Piétu, Guilloteau & Dutrey (2005) and Panić et al. (2008) show that the gas-to-dust ratios in the AB Aur and HD 169142 disks are consistent with the interstellar medium value of 100.

Rotational lines of other molecules further constrain the physical structure as

well as the chemistry of the outer disk. The first results were obtained using single-dish telescopes, measuring the globally averaged properties, and showed that other molecules including HCO^+ and H_2CO were also strongly depleted as much as, if not more than, CO in classical T Tauri disks (Dutrey, Guilloteau & Guelin 1997; Thi, van Zadelhoff & van Dishoeck 2004; van Zadelhoff et al. 2001). Photodissociated products such as CN were relatively abundant, however, which led to the picture of a photon dominated region at the surface of a warm intermediate layer with $T \sim 20 - 40$ K, $n(\text{H}_2) \sim 10^6 - 10^8 \text{ cm}^{-3}$, sitting on a cold, highly depleted midplane. The details in this picture are being filled in as new lines and species are detected (e.g., Henning et al. 2010).

Thi, van Zadelhoff & van Dishoeck (2004) found a high deuterium fraction in TW Hydra, similar to values seen in dense cores and attributed to cool temperatures and high CO depletion (Caselli et al. 1999). Interferometric imaging resolves the D/H ratio, shows that it varies from ~ 0.01 to ~ 0.1 across the disk and peaks at ~ 70 AU radius (Qi et al. 2008), a result with implications for understanding the high D/H ratio in comets and the delivery of water to Earth (Ehrenfreund & Charnley 2000). The suite of molecular line maps in Figure 4 directly shows the decrease in DCO^+ 3-2 intensity at the center of the disk where the CO depletion is lower due to the higher temperatures. Deuterated species, in particular H_2D^+ , and other molecules with very low condensation temperatures such as N_2H^+ should reveal the physical conditions and kinematics of the disk midplane in the outer disk. The lines are weak but H_2D^+ has been detected in one, possibly two, sources by Ceccarelli et al. (2004) and N_2H^+ has been detected in several disks (Dutrey et al. 2007, Öberg et al. 2010, Qi et al. 2003). The cool temperatures of T Tauri star disks lead to CO freeze out and a richer chemistry that is absent in warmer Herbig AeBe disks (Öberg et al. 2010). The reader is referred to Bergin (2009) for a more exhaustive discussion of disk chemistry.

The full analysis of the many species and lines now detected in protoplanetary disks requires sophisticated models to handle the physical, thermal, and chemical structure and the feedback of each of these on each other (e.g., Woitke, Kamp & Thi 2009). The complexity is such that, for T Tauri stars at least, there is no simple prescription for the gas mass. However, these observations provide substantial information about the disk structure and complement the broadband dust measurements. Disks have a dynamic atmosphere above a cool midplane: the temperature increases with height, the phase changes from molecular to atomic to ionized, and dust grains undergo sublimation and condensation of icy mantles as they move throughout.

Finally, as this review is being written, the first results are coming in from *Herschel* and its far-infrared spectrometers. The $[\text{OI}] 63 \mu\text{m}$ line is generally the strongest line in this regime and widely detected (Mathews et al. 2010). Combined with ground based CO measurements, it provides strong constraints on the gas mass (Thi et al. 2010). Multiple transitions of this and other species can be detected in some sources and allow the excitation conditions of the gas to be determined (Sturm et al. 2010). However, the weakness of H_2O lines at sub-millimeter wavelengths indicates that almost all the water is frozen onto icy mantles around large dust grains that have settled to the midplane (Bergin et al. 2010). In *Herschel*'s 3 year lifetime, we expect to learn much more about the gaseous content of disks in the giant planet-forming zone.

4.5 Dependence on stellar mass

Disks are observed around a wide range of stars from very low mass to intermediate mass Herbig Ae/Be stars. Infrared excesses from disks around brown dwarfs are also detected at a similar frequency to stars (Luhman et al. 2005) and masses for a handful have been measured from millimeter wavelength measurements (Scholz, Jayawardhana & Wood 2006). The relationship between disk and stellar properties informs models of disk formation and evolution.

Higher mass stars require more material to pass through a disk and we might therefore expect to see a positive correlation between disk mass and stellar mass (e.g., Natta, Grinin & Mannings 2000). Figure 5 compiles (sub-)millimeter measurements of Class II YSO disks from the literature (Acke et al. 2004; Alonso-Albi et al. 2009; Mannings & Sargent 2000; Natta, Grinin & Mannings 2000; Scholz, Jayawardhana & Wood 2006) and shows that there is a large scatter, ~ 0.5 dex, but confirms that disk masses tend to be lower around low mass stars such that the ratio, $M_d/M_* \sim 0.01$.

The relationship breaks down for the most massive stars. There is no (sub-)millimeter detection of a disk around an optically visible O star. The limits on the sensitive Orion proplyd survey provide the most stringent constraints to date, $M_d/M_* \lesssim 10^{-4}$ for $M_* \geq 10 M_\odot$ (Mann & Williams 2009b). This may be due to very high photoevaporation rates so that disks are not detectable by the time an O star is optically visible or due to an altogether different star formation mechanism (Zinnecker & Yorke 2007).

Disk size measurements, whether from optical observations of Orion proplyds (Vicente & Alves 2005) or millimeter visibilities of Ophiuchus disks (Andrews et al. 2009, 2010b), are of a restricted range of stellar masses, $M_* \simeq 0.3 - 2 M_\odot$, and do not follow a clear trend. Moreover, Panić & Hogerheijde (2009) argue that observations of Herbig Ae/Be stars at millimeter wavelengths have been biased toward large, bright disks. *ALMA* will soon provide the resolution and sensitivity required to measure disk radii in a more representative sample.

Disk structure does appear to be dependent on stellar mass, at least for low mass stars. Szűcs et al. (2010) find that relatively blue mid-infrared colors imply smaller scale heights for disks around very low mass stars than low mass stars in the same star-forming region. It is harder to make a direct comparison to higher mass Herbig Ae/Be stars in other regions because of the difficulty in distinguishing initial conditions from evolution due to grain growth and settling.

4.6 Section summary

- Disk masses are best measured from (sub-)millimeter observations of thermal continuum emission from dust. Substantial, and uncertain, corrections are required for the grain size distribution and gas-to-dust ratio.
- Assuming an ISM gas-to-dust ratio of 100 and ignoring the mass in bodies larger than 1 mm, the median mass of protoplanetary disks around Class II YSOs with spectral types GKM is $5 M_{\text{Jup}}$.
- Protoplanetary disks have power law surface density profiles with an exponential taper that produces a soft edge anywhere from 20 to 200 AU from the star. The power law index is approximately -1 but is extrapolated and highly uncertain within the central ~ 20 AU.
- Surface densities are generally below the threshold for gravitational instability and velocity profiles are Keplerian.

- Mid-infrared through millimeter spectroscopy reveals a warm molecular layer with PDR-like chemistry that is strongly dependent on the stellar luminosity and a cold midplane depleted of molecules.
- From brown dwarfs to B stars, disk masses scale with the stellar mass. The median ratio is about 1% but there is a large dispersion, ± 0.5 dex.

5 DISK LIFETIMES

One of the most fundamental parameters on disk evolution studies is the lifetime of the disk itself. This is not only because it reflects the relevant time scale of the physical processes driving the dissipation of the disk, but also because it sets a limit on the time available for planet formation.

Even though the mass of the gas initially dominates that of the dust by two orders of magnitude in primordial disks, the dust is much easier to observe and thus most of the constraints on the lifetimes of circumstellar disks have been obtained by observing the thermal emission of the dust grains. These particles absorb stellar light and reradiate mostly in the $1\,\mu\text{m}$ to $1\,\text{mm}$ range. Because the temperature of the dust decreases with the distance from the central star, different wavelengths trace different disk radii (for a given stellar luminosity). In what follows, we summarize the observational constraints provided by near-infrared and mid-infrared observations, mostly from *Spitzer*, which has performed the most sensitive and comprehensive surveys of disks in star-forming regions to date. Toward the end of the section, we also briefly discuss current constraints on gas dispersal time scales.

5.1 Near-infrared results: the inner disk

Because there is a very well established correlation between the presence of near-infrared excess ($1 - 5\,\mu\text{m}$) and the occurrence of spectroscopic signatures of accretion (Hartigan, Edwards & Ghandour 1995), it is possible to investigate the lifetime of inner accretion disks ($R \lesssim 0.1\,\text{AU}$) by studying the fraction of stars with near-infrared excess as a function of stellar age. Early studies of nearby star-forming regions found that 60 – 80% of stars younger than 1 Myr present measurable near-infrared excesses, and that no more than 10% of stars older than 10 Myr do so (e.g., Strom et al. 1989). Given the large uncertainties associated with model-derived stellar ages, it has been argued that individual star-forming regions lack the *intrinsic* age spread necessary to investigate disk lifetimes from individually derived ages and the apparent age dispersion is mostly driven by the observational uncertainties (Hartmann 2001). However, similar studies based on the disk frequencies in clusters with a range of *mean* ages (Haisch, Lada & Lada 2001; Hillenbrand 2005) have led to essentially the same result: the frequency of inner accretion disks steadily decreases from < 1 to ~ 10 Myr (e.g., see Figure 2 in Wyatt (2008)).

The inner disk fractions observed in both young stellar clusters and in the distributed population of pre-main sequence stars in star-forming regions are consistent with median disk lifetimes of between 2 and 3 Myr. The decrease has also been modeled as an exponential with e-folding time 2.5 Myr (Mamajek 2009). The uncertainty in this number is mainly due to the difficulty in determining stellar ages accurately at these early times, and the uncertain duration of

star formation in a cluster. There is also a wide dispersion in the lifetimes: some objects lose their inner disks at a very early age ($\lesssim 1$ Myr), even before they become optically revealed and can be accurately placed in the Hertzsprung-Russell diagram, whereas other objects retain their accretion disks for up to 10 Myr.

5.2 Spitzer results: the planet-forming regions of the disk

Because only circumstellar dust very close to the star ($R \lesssim 0.1$ AU) becomes hot enough to be detectable in the near-infrared, observations at these wavelengths provide no information on the presence of circumstellar material beyond ~ 0.5 AU. As a result, disk lifetime studies based on near-infrared excesses always left room for the possibility that stars without near-infrared excess had longer-lived outer disks with enough material to form planets at radii that could not be detected at these short wavelengths.

IRAS and *ISO* both had the appropriate wavelength range to study the planet-forming regions of the disk ($R \sim 0.5 - 20$ AU) but lacked the sensitivity needed to detect all but the strongest mid- and far-infrared excesses in low-mass stars at the distances of the nearest star-forming regions. During its 6-year cryogenic mission, *Spitzer* provided, for the first time, the wavelength coverage and the sensitivity needed to detect very small amounts of dust in the planet-forming regions of thousands of YSOs. The wealth of data made available by *Spitzer* has not only firmly established the dissipation time scale of primordial disks, but also made it possible to address second-order questions such as the effect of stellar mass, multiplicity, and external environment on disk lifetimes.

5.2.1 STELLAR CLUSTERS AND ASSOCIATIONS Just as was done for the inner disk with near-infrared studies, the dissipation time scale of regions farther out in the disk can be investigated by observing the fraction of stars that show mid-infrared excesses in clusters of different ages. Reaching the stellar photospheres of all the targets is needed to unambiguously establish the fraction of them that have an infrared excess indicating the presence of a disk. However, while at $8.0 \mu\text{m}$ *Spitzer* was able to detect the stellar photospheres of solar-type stars at distances of up to 1 kpc, at longer wavelengths it was only sensitive enough to detect solar-type photospheres within ~ 200 pc. Because there are very few stellar clusters within 200 pc, we focus on the results from IRAC (3.6 to $8.0 \mu\text{m}$) observations.

Comparing the disk fractions of stellar clusters presented by different *Spitzer* studies is not completely straightforward as the methods used to decide which objects are members of the cluster, the disk identification criteria, sensitivities, and ranges of stellar masses considered vary from study to study.

Very young embedded clusters (age ≤ 1 Myr) such as Serpens and NGC 1333 show disk fractions of the order of 70 to 80% (Gutermuth et al. 2008, Winston et al. 2007). This implies that pre-main sequence stars without a disk, showing photospheric IRAC fluxes, are seen even in extremely young star-forming regions. Clusters in the 2 – 3 Myr range, such as IC 348 and NGC 2264, show IRAC disk fractions of the order of 40 to 50% (Lada et al. 2006, Sung, Stauffer & Bessell 2009), whereas regions with estimated ages around ~ 5 Myr, such as Upper Scorpius and NGC 2362 exhibit disk fractions that are already below 20%. By $\sim 8 - 10$ Myr old, primordial disks with IRAC excesses become exceedingly rare as attested by their very low incidence ($\lesssim 5\%$) in regions such as the TW Hydra, σ Ori, and NGC 7160 associations (Hernández et al. 2007, Sicilia-Aguilar et al.

2006).

The main results on disk lifetimes from IRAC studies of young stellar clusters listed above are indistinguishable from those obtained by pre-*Spitzer* near-infrared studies. This is not too surprising considering that IRAC wavelengths only trace regions inward of ~ 5 AU around solar type stars. These regions are further out in the disk than those traced by near-infrared observations, but still exclude the bulk of the disk material. Thus, the question remains: can primordial outer disks ($R > 5$ AU) survive beyond 10 Myr? To address this question, we must turn to the longer wavelength camera, MIPS, on *Spitzer*, and studies of star-forming regions within 200 pc, where $24\ \mu\text{m}$ observations are sensitive enough to reach the stellar photosphere of their targets and unambiguously identify the presence of a disk.

5.2.2 THE DISTRIBUTED POPULATION OF PRE-MAIN SEQUENCE STARS Firmly establishing the longevity of primordial disks was one of the central goals of two *Spitzer* Legacy Programs: “From Molecular Cores to Planet-forming Disks” (cd2: Evans et al. 2003) and “Formation and Evolution of Planetary Systems” (FEPS: Meyer et al. 2006).

As part of the c2d project, *Spitzer* observed over 150 WTTS associated with the Chameleon, Lupus, Ophiuchus, and Taurus star-forming regions, all within 200 pc of the sun. As one of the main goals was to establish whether the outer disk could significantly outlive the inner disk, the c2d sample of WTTS was mostly composed of X-ray identified and spectroscopically confirmed pre-main sequence stars without evidence for an inner accretion disk.

Results from the c2d project (Cieza et al. 2007, Padgett et al. 2006, Wahhaj et al. 2010) show that $\sim 80\%$ of young WTTS present $24\ \mu\text{m}$ fluxes consistent with bare stellar photospheres. Because $24\ \mu\text{m}$ observations are sensitive to very small amounts of micron sized dust ($\ll 1 M_{\oplus}$) out to tens of AU from the central star, this suggests that once accretion stops and the inner disk dissipates, the entire disk goes away very quickly. The fraction of c2d WTTS with $24\ \mu\text{m}$ excesses is a function of stellar age. Approximately 50% of the WTTS younger than $\lesssim 1 - 2$ Myr do not have a disk, suggesting that a significant fraction of the entire pre-main sequence population lose their disks by an age of ~ 1 Myr. However, none of the WTTS in the c2d sample older than ~ 10 Myr has a detectable disk. Also, many of the WTTS disks have very low fractional disk luminosities, ($L_{\text{disk}}/L_{\star} < 10^{-3}$), and are thus more consistent with optically thin debris disks than with primordial disks.

Very similar results were obtained by the FEPS project, which observed 314 solar-type stars with a median distance of 50 pc and ages ranging from 3 Myr to 3 Gyr. The youngest age bin in the FEPS study included 34 targets younger than 10 Myr and a mean age of ~ 5 Myr. They find that only 4 out of those 34 targets had optically thick primordial disks, whereas 5 of them had optically thin debris disks. The second youngest bin in their study had 49 targets with estimated ages in the 10 to 30 Myr range. In this age bin, they identified 9 debris disk and only one primordial disk (Carpenter et al. 2009). The only target with a primordial disk in this age range was PDS 66, a member of the Lower Centaurus Crux association with an estimated, but uncertain, age of 12 Myr (Preibisch & Mamajek 2008).

Both the c2d and FEPS results strongly suggest that, while there is a wide dispersion on disk lifetimes, ~ 10 Myr is a firm upper limit for the longevity

of primordial circumstellar disks around solar-type stars. They also show that there is a significant overlap in the age distributions of primordial and debris disks. Exactly how and when protoplanetary disks evolve into planetary debris disks remains an open question and is discussed in §6.4.

5.3 Dissipation timescale

The fact that very few objects lacking near-infrared excess show mid-infrared excess emission implies that, once accretion stops and the inner disk clears out, the entire disk dissipates very rapidly. This is also supported by (sub-)millimeter observations (André & Montmerle 1994, Andrews & Williams 2005, 2007a) showing a very strong correlation between the detectability of a disk at these long wavelengths and presence of an inner accretion disk. This implies that the vast majority of pre-main sequence stars in any given population are either accreting CTTS with excess emission extending all the way from the near-infrared to the sub-millimeter or have bare stellar photospheres. Based on the small incidence of objects lacking an inner disk that have evidence of an outer disk, the dissipation timescale of the entire primordial disk once accretion stops has repeatedly been estimated to be $\lesssim 0.5$ Myr (e.g., Cieza et al. 2007, Skrutskie et al. 1990, Wolk & Walter 1996). This finding, that circumstellar material can survive at all radii ($R \lesssim 0.1 - 200$ AU) for several Myr, while later the dissipation of the entire disk occurs in a much shorter timescale is known as the “two-time-scale” problem. Disk evolution models combining viscous accretion with photoevaporation (e.g., Alexander, Clarke & Pringle 2006a,b) have successfully been able to reproduce this behavior (see §6.2).

5.4 Dependence on stellar mass

Young stellar clusters and associations provide an excellent opportunity to investigate disk lifetimes as a function of stellar mass as they contain large samples of mostly coeval stars spanning a large range of stellar masses. In their study of the 5 Myr old Upper Scorpius OB association, Carpenter et al. (2006) obtained 4.5, 8.0 and $16 \mu\text{m}$ photometry of 204 members with masses ranging from ~ 0.1 to $20 M_{\odot}$. They find that while $\sim 20\%$ of their 127 K and M-type targets (masses $\sim 0.1 - 1.2 M_{\odot}$) are surrounded by optically thick, primordial circumstellar disks, none of their 30 F and G-type stars (masses $\sim 1.2 - 1.8 M_{\odot}$) had any evidence for a disk at wavelengths $\leq 16 \mu\text{m}$.

An almost identical result was obtained by Dahm & Hillenbrand (2007) in the also 5 Myr old cluster NGC 2362. They found a total IRAC disk fraction of $\sim 20\%$ (7% of strong excesses and 12% of weaker excesses) among 220 stars with estimated masses below $1.2 M_{\odot}$ and a complete absence of IRAC excesses among 33 stars with estimated masses above $1.2 M_{\odot}$. MIPS observations of NGC 2362 (Currie et al. 2009) and other 5 Myr old clusters such as λ Orionis (Hernández et al. 2009) do show $24 \mu\text{m}$ excesses for objects with masses above $1.2 M_{\odot}$, but they are all consistent with the optically thin emission expected from debris disks. Overall, the *Spitzer* results suggest that, though primordial circumstellar disks can last for up to 10 Myr around solar and lower-mass stars, disk lifetimes are a factor of ~ 2 shorter around higher mass objects. The higher accretion rates and radiation environment are likely to be responsible for the shorter disk lifetimes in higher mass stars (Calvet et al. 2005, Garcia Lopez et al.

2006, Hillenbrand 2008).

At the lower end of the mass distribution, the statistics are much poorer. The disk fractions of brown dwarfs in relatively young regions (age 1 – 3 Myr) such as Taurus, Chamaeleon I, and IC 348 has been found to be between 40 and 50% with statistical uncertainties as large as 10 to 20% (Guieu et al. 2007, Luhman et al. 2005, Monin et al. 2010). For the 5 Myr Upper Scorpius region, the reported values range from $37 \pm 9\%$ (Scholz et al. 2007) to $11^{+9}_{-3.3}\%$ (Riaz, Lodieu & Gizis 2009). Also, 3 of the 5 known brown dwarfs in the 10 Myr old TW Hydrae association have infrared excesses indicating the presence of a disk (Riaz & Gizis 2008). Taken together, these observations suggest that the dissipation time scales of disks around substellar objects are at least as long as those of solar-mass stars, although significantly longer disk lifetimes cannot be ruled out based on the available data.

5.5 Gas dispersal

CO observations toward disks that are warm enough to prevent freeze-out hint at a decrease in the gas-to-dust ratio with evolutionary class (Chapillon et al. 2010; Dutrey, Guilloteau & Simon 2003). Unlike dust, however, there is no generic tracer of the gas mass in young disks (see §4.4.2) and systematic studies of gas dispersal with stellar age has been studied by observing accretion indicators.

Using the equivalent widths and velocity profiles of the H α line to identify accretors, Fedele et al. (2010) recently studied the fractions of accreting objects in stellar clusters with ages in the 1–50 Myr range. They find no accreting objects in the clusters older than 10 Myr down to an accretion sensitivity estimated to be $\sim 10^{-11} M_{\odot} \text{ yr}^{-1}$. They also find that, in most clusters, the fraction of accreting stars is systematically lower than the fraction of objects with *Spitzer* excesses in IRAC bands. This is expected as $\sim 20\%$ of non-accreting pre-main sequence stars (i.e., WTTS) have IRAC excesses (Cieza et al. 2007, Damjanov et al. 2007, Wahhaj et al. 2010), while the fraction of accreting pre-main sequence stars (i.e., CTTS) lacking IRAC excesses is significantly smaller, of the order of $\lesssim 2\text{--}5\%$ (e.g., Cieza et al. 2010, Muzerolle et al. 2010).

Accretion only shows the presence of gas in the inner disk. Consequently, our current understanding of the time scale of the gas dispersal is in an analogous situation to that of the dust dissipation prior to *Spitzer*: although the longevity of gaseous inner disks is well established to be $\lesssim 10$ Myr, the possibility of significant amounts of gas remaining for longer period of times at larger radii still exists. However, according to the “UV-switch” model (Alexander et al., 2006), photoevaporation removes all circumstellar gas very quickly ($\ll 1$ Myr) once accretion stops (see §6.2). *Herschel* studies currently underway of sensitive gas tracers, such as the $63.2 \mu\text{m}$ [O I] line, should be able to test this prediction.

5.6 Environmental influences

Protoplanetary disks are detected in a range of environments from low mass, sparsely populated molecular clouds to massive, dense stellar clusters. In nearby, well studied, low mass star-forming regions, there is a remarkable similarity in the average disk properties from region to region as demonstrated from mid-infrared colors (Fang et al. 2009) and spectra (Furlan et al. 2009) and also in their mass distributions and sub-millimeter colors (Andrews & Williams 2005, 2007a). This

is not unexpected given that disk sizes are orders of magnitude smaller than typical star-to-star distances except perhaps in the densest parts of very young protoclusters and disruptive encounters with a passing star is not a common evolutionary determinant (Sclally & Clarke 2001). Gravitational perturbations have a strong impact on disk evolution, however, in close binary or multiple systems.

The median disk lifetime of 2–3 Myr (discussed in §5) is derived from surveys of many clusters. There is a rather small dispersion in the disk fraction at any given age despite the different cluster sizes and whether or not they contain massive stars. These mid-infrared observations are unable to measure the properties of the outer parts of the disk, however, which are more susceptible to external influences. Here, we discuss the influences of binary stars, massive stars, and also metallicity on disk lifetimes.

5.6.1 DYNAMICAL DISRUPTION IN BINARIES About half of field stars are in binary or higher order multiple systems (Raghavan et al. 2010). The orbital resonances in these systems have a profound influence on disk evolution. Artymowicz & Lubow (1994) show that (coplanar) disks around each star in a binary system are truncated at the outer edge, and a circumbinary ring about both stars are truncated at the inner edge. As a rough guide for near circular orbits with semi-major axis a , the circumprimary disk is limited in size to $\sim a/2$ and the circumbinary disk’s inner edge is $\sim 2a$. Higher eccentricities lead to greater disk erosion.

There are a few resolved disk images that confirm this general pattern. GG Tau is perhaps one of the best studied circumbinary disks with an inner radius of 180 AU (Guilloteau, Dutrey & Simon 1999) although it appears to be bigger than expected given the $a = 32$ AU, $e = 0.34$ binary orbit (Beust & Dutrey 2005). UY Aur (Duvert et al. 1998) and CoKu Tau 4 (Ireland & Kraus 2008) are additional examples of primordial circumbinary disks but they appear to be rare exceptions rather than the rule. Outwardly truncated circumstellar disks, only a few tens of AU in diameter, have also been detected in binary systems, L1551-IRS5 (Rodríguez et al. 1998), GQ Lup (Dai et al. 2010), HD 98800 and Hen 3-600 (Andrews et al. 2010a).

High resolution speckle imaging studies searching for a connection between binaries and premature disk dissipation initially yielded mixed and inconclusive results. Ghez, Neugebauer & Matthews (1993) surveyed ~ 70 pre-main sequence stars in Taurus and Ophiuchus and concluded that the incidence of close binaries ($a < 50$ AU) in WTTS is enhanced with respect to that of CTTS. This was not confirmed, however, by subsequent larger studies in Taurus (Köhler & Leinert 1998, Leinert et al. 1993). Yet a survey of ~ 160 pre-main sequence stars in Ophiuchus by Ratzka, Köhler & Leinert (2005) showed that YSOs with infrared excesses tend to have fewer companions and are at smaller projected separations than diskless YSOs.

Here, again, the uniformity and sensitivity of *Spitzer* studies have improved our understanding of the situation. Cieza et al. (2009) combined the results from several multiplicity surveys of pre-main sequence stars with *Spitzer* data of four star-forming regions and showed that the distribution of projected separations of systems with mid-infrared excesses are in fact significantly different from that of systems without. Binaries with projected separations less than 40 AU are half as likely to possess a disk than those with projected separations in the 40 – 400 AU

range. Duchêne (2010) finds a similar result with a somewhat smaller sample. (Sub-)millimeter fluxes are also known to be lower for similarly close binaries indicating that the bulk of the disk has been lost (Andrews & Williams 2005, Jensen, Mathieu & Fuller 1994, 1996, Osterloh & Beckwith 1995).

Even though several factors (e.g., the incompleteness of the census of close binaries, the use of unresolved disk indicators, and projection effects) tend to weaken its observable signature, the effect of multiplicity on disk lifetimes could be very strong. The distribution of physical separations, a , in solar-type pre-main sequence binaries is expected to peak around 30 AU as in field stars (Duquennoy & Mayor 1991, Raghavan et al. 2010). Hence the disks around individual stars in most binary systems should have truncation radii of the order of $(0.3-0.5)a \sim 10-15$ AU (Papaloizou & Pringle 1977). These truncation radii are about an order of magnitude smaller than the typical radii of disks around single stars (see §4.2). For an accretion disk with $\gamma = 1$ (see §4.3.1), the viscous time scales linearly with radius and is therefore also about an order of magnitude smaller. This implies that the lifetimes of disks around the individual components of most binary systems should be $\sim 10\%$ of those of single stars or about 0.3 Myr. These very short lifetimes for the stars in medium-separation binary systems may explain both the presence of very young diskless stars and the large dispersion in disk dissipation time scales.

5.6.2 PHOTOEVAPORATION BY MASSIVE STARS Most stars form in large clusters with hundreds if not thousands of stars (Lada & Lada 2003, McKee & Williams 1997). Such large stellar groups are highly likely to contain an O star which bathes neighboring stars and their disks in a UV radiation field that may be several orders of magnitude above the interstellar average. The effect is to rapidly erode the more loosely bound outer parts of a disk.

The spectacular *Hubble* images of photoevaporating disks embedded in small ionized cocoons (Bally, O'Dell & McCaughrean 2000) make a stunning contrast to the large Taurus disks in their more benign low radiation environment (Padgett et al. 1999). The pictures are somewhat misleading, however, in that the central regions of Orion disks are not strongly affected. Except for disks very close to the O stars where ionizing photons directly impinge on the disk surface, the disk develops a thick photon dominated region with a temperature $\sim 10^3$ K. The corresponding thermal velocity, $\sim 3 \text{ km s}^{-1}$, implies that gas is bound to the central star for radii $\lesssim 100$ AU (Adams et al. 2004). Gas pressure can cause mass loss at smaller radii but the evaporation timescale within solar system scales, < 50 AU, is tens of Myr (Clarke 2007).

The comparison of disk masses in Orion with Taurus and Ophiuchus in Figure 1 illustrate these points. There is a deficit of massive disks at the center of the Trapezium Cluster but such disks would likely have been the largest and therefore the most susceptible to photoevaporation by the O6 star, θ^1 Ori C. The discrepancy at the upper end of the mass distribution is roughly consistent with the smaller median size of Orion proplyds compared to Taurus disks. Further, the fraction of disks with at least a MMSN, $10 M_{\text{Jup}}$, within 60 AU is similar, $\sim 11-13\%$, in Taurus, Ophiuchus, and Orion and, incidentally, comparable to the detection rate of Jupiter mass extrasolar planets (Mann & Williams 2009b).

More massive disks are found further away from the center of the Trapezium Cluster (Eisner et al. 2008, Mann & Williams 2009a), and the disk mass distribution of the full Orion region more closely resembles those in Taurus and Ophiuchus

(see Figure 1). The large difference in mass between the most massive disks in and out of the cluster center compared to the difference in stellar density rules out stellar encounters as the cause (Olczak, Pfalzner & Spurzem 2006).

VLA and *SMA* observations do not currently have sufficient sensitivity to study more distant regions. However, *Hubble* and *Spitzer* observations find morphological features similar to the Orion proplyds in other massive star-forming regions (Balog et al. 2006; Smith, Bally & Morse 2003). Hernández et al. (2008) find that the γ Velorum cluster has a low fraction of sources with infrared excesses for its age and consider disk photoevaporation as a possibility but also note the large uncertainty in the cluster age. The disk fraction decreases by about a factor of 2 within the central 0.5 pc of the Rosette nebula (Balog et al. 2007) and the central 1 pc of S Monoceros (Sung, Stauffer & Bessell 2009) but the statistics are limited by small numbers. External evaporation can only remove the inner disk on such short timescales with very strong radiation fields that directly ionize the disk and boil it off at $\sim 10^4$ K (Adams et al. 2004, Clarke 2007). It is hard to reconcile this with a parsec-scale sphere of influence of a massive star unless the stellar orbits are highly eccentric (Störzer & Hollenbach 1999).

Balog et al. (2008) show that the *Spitzer* 24 μ m dusty tails in these regions are not detected in $\text{Pa}\alpha$ and are effectively gas-free. They suggest that photoevaporation removes the gas very quickly but that a dusty reservoir is replenished by the collisions of large bodies left behind in the disk. Throop & Bally (2005) consider the rapid enhancement of the dust-to-gas ratio in photoevaporating disks as a potential trigger for planetesimal formation. External evaporation has also been considered as a possible explanation of the steep drop in the surface density of Kuiper Belt Objects beyond 50 AU (Jewitt, Luu & Trujillo 1998).

5.6.3 THE EFFECT OF METALLICITY The effect of the metallicity, or the initial dust-to-gas content, on the evolution of protoplanetary disks has not been well studied, at least at the early stages. It is known that the metallicity of the host star is strongly correlated with the presence of hot Jupiters (Valenti & Fischer 2005). This may be due to an enhanced rate of planetesimal formation (Johansen, Youdin & Mac Low 2009) but longer disk lifetimes may also play a role. In a small sample, D’Orazi et al. (2009) do not find any significant difference in the metallicities of Taurus and Orion WTTS or CTTS. However, Yasui et al. (2009) showed the inner disk fraction, as measured by near-infrared excesses, is significantly smaller in low metallicity clusters at the edge of the Galaxy. Yasui et al. (2010) extend this work to other distant, low metallicity clusters of different ages and find a median disk lifetime, < 1 Myr. They suggest a strong dependence of the lifetime on metallicity, which is in qualitative agreement with photoevaporative models of disk evolution (Ercolano & Clarke 2010).

5.7 Section summary

- Disk lifetimes have a median between 2 and 3 Myr but vary from less than 1 Myr to a maximum of 10 Myr. Multi-wavelength observations show that the dissipation timescale is very similar at all radii.
- Circumstellar disks dissipate faster around high-mass stars than around solar mass stars. Very low mass-stars and brown dwarfs have disk lifetimes at least as long as, and likely longer than, those of solar mass stars.
- Disk lifetimes are significantly shorter around medium separation binaries

($a \sim 5 - 100$ AU).

- Photoevaporation from massive stars erodes the outer parts of disks but generally leaves their interiors ($\lesssim 50$ AU) intact. The lifetimes and masses are only significantly reduced for disks that lie within a few tenths of a parsec from an O star.
- Disks in low metallicity environments at the edge of the Galaxy have median lifetimes < 1 Myr, which are substantially shorter than in the Solar neighborhood.

6 DISK EVOLUTION

Understanding the physical processes that drive the evolution of primordial circumstellar disks, as they evolve from optically thick to optically thin, is crucial for our understanding of planet formation. Disks evolve through various processes, including viscous accretion, dust settling and coagulation, dynamical interactions with (sub-)stellar companions and forming planets, and photo-evaporation by ultraviolet and X-ray radiation. In this section we summarize the models and observational constraints for the different processes that control the evolution of primordial circumstellar disks.

6.1 Viscous transport

To first order, the evolution of primordial disks is driven by viscous transport. The accretion from the inner disk onto the star is relatively well understood and well constrained observationally. The large velocity widths, intensities, and profiles of emission lines such as $H\alpha$, $Br\gamma$ and $Ca II$ can be successfully reproduced by magnetospheric accretion models (Muzerolle, Calvet & Hartmann 1998). The physical mechanisms that drive the radial transport across the disk are reviewed by Armitage (2010).

Viscous evolution models are broadly consistent with the observational constraints for disk masses and sizes, and the decrease in accretion rate over time (Hartmann et al. 1998, Hueso & Guillot 2005). However, pure viscous evolution models also predict a smooth, power-law evolution of the disk properties. This secular disk evolution is inconsistent with the very rapid disk dissipation that usually occurs after a much longer disk lifetime (i.e. the “two-time-scale” problem). Viscous evolution models also fail to explain the variety of SEDs observed in the transition objects discussed in §7. These important limitations of the viscous evolution models show that they are in fact just a first-order approximation of a much more complex evolution involving several other important physical processes.

6.2 Photoevaporation by radiation from the central star

Together with viscous accretion, photoevaporation is one of the main mechanisms through which primordial circumstellar disks are believed to lose mass and eventually dissipate. Photoevaporation can be driven by energetic photons in the far-ultraviolet (FUV: $6\text{ eV} < h\nu < 13.6\text{ eV}$), extreme-ultraviolet (EUV: $13.6\text{ eV} < h\nu < 0.1\text{ keV}$) and X-ray ($h\nu > 0.1\text{ keV}$) energy range. Photons in each energy range affect the disks in different ways, and the relative importance of FUV,

EUV, and X-ray photoevaporation is still not well understood. Photoevaporating photons can originate both from nearby massive stars and from the central star itself. The former scenario was discussed in §5.6.2 and here we focus on the latter.

Early photoevaporation models focused on the effect of ionizing EUV radiation (e.g., Hollenbach et al. 1994) on circumstellar gas around early-type stars. Later disk evolution models, known as “UV-switch” models, combine viscous evolution with photoevaporation by EUV photons (Alexander, Clarke & Pringle 2006a,b; Clarke, Gendrin & Sotomayor 2001) to tackle the “two-time-scale” problem of T Tauri evolution (i.e., the sudden dispersion of the entire disk after much longer disk lifetimes, see §5.3). According to these models, extreme ultraviolet (EUV) photons originating at the stellar chromospheres of low-mass stars ionize and heat the circumstellar hydrogen to $\sim 10^4$ K. Beyond a critical radius, ~ 10 AU for solar mass stars, the thermal velocity of the ionized hydrogen exceeds its escape velocity and the material is lost in the form of a wind.

At early stages in the evolution of the disk, the accretion rate dominates over the evaporation rate and the disk undergoes standard viscous evolution: material from the inner disk is accreted onto the star, while the outer disk behaves as a reservoir that resupplies the inner disk, spreading as angular momentum is transported outwards. Later on, as the accretion rate drops to the photoevaporation rate, $\sim 10^{-10} - 10^{-9} M_{\odot} \text{ yr}^{-1}$ in the models, the outer disk is no longer able to resupply the inner disk with material. At this point, the inner disk drains on a viscous timescale ($\lesssim 10^5$ yr) and an inner hole of a few AU in radius is formed in the disk. The inner disk edge is now directly exposed to the EUV radiation and the disk rapidly photoevaporates from the inside out. Thus, the UV-switch model naturally accounts for the lifetimes and dissipation timescales of disks as well as for SEDs of some pre-main sequence stars suggesting the presence of large inner holes.

Recent photoevaporation models include X-ray (Owen et al. 2010, e.g.,) and/or FUV irradiation (Gorti, Dullemond & Hollenbach 2009; Gorti & Hollenbach 2009, e.g.,) in addition to the EUV photons. Because X-rays and FUV photons are able to penetrate much larger columns of neutral gas than EUV photons, they are able to heat gas that is located both deeper in the disk and at larger radii. Thus, while EUV induced photoevaporation is restricted to the inner few AU of the disk, X-rays and FUV photons can operate at tens of AU from the star.

EUV+X ray and FUV+X-ray models show a similar qualitative behavior to photoevaporation by EUV alone, but also several important differences (Armitage 2010). Most notably, they predict photoevaporation rates of the order of $10^{-8} M_{\odot} \text{ yr}^{-1}$, which are two orders of magnitude greater than pure EUV photoevaporation models. Consequently an inner hole forms early in a disk’s accretion history. As a result, EUV+X ray and FUV+X-ray models predict a significant population of pre-main sequence stars with relatively massive ($\gtrsim 10 M_{\text{Jup}}$) disks with large inner holes and no, or very little, accretion. However, observations have shown that disks around WTTS tend to have much lower masses, $\lesssim 1 - 2 M_{\text{Jup}}$ (Andrews & Williams 2005, 2007a, Cieza et al. 2010, 2008). This suggests that, in reality, the photoevaporation rates and disk masses are lower than those predicted by Gorti, Dullemond & Hollenbach (2009) and Owen et al. (2010) when the inner hole is initially formed and that the quantitative predictions of current photoevaporation models should be taken with caution.

6.3 Grain growth and dust settling

Even though solid particles only represent 1% of the initial mass of the disk, understanding their evolution is of utmost interest for disk evolution and planet formation studies. Solids not only dominate the opacity of the disk, but also provide the raw material from which the terrestrial planets and the cores of the giant planets (in the core accretion model) are made. Although viscous accretion and the photoevaporation processes discussed above drive the evolution of the gas, other processes operate on the solid particles, most importantly, grain growth and dust settling.

Grain growth and dust settling are intimately interconnected processes. Gas motions differ slightly from Keplerian motions due to pressure. Small ($r \sim 0.1 \mu\text{m}$) grains have a large surface-to-mass ratio and are swept along with the gas. As grains collide and stick together, their surface-to-mass ratio decreases and their motions decouple from the gas. They therefore suffer a strong drag force and settle toward the midplane. This increases the density of dust in the interior of the disk, which accelerates grain growth, and results in even larger grains settling deeper into the disk. If this process were to continue unimpeded, the end result would be a perfectly stratified disk with only small grains in the disk surface and large bodies in the midplane. However, because circumstellar disks are known to be turbulent, some degree of vertical stirring and mixing of grains is expected (Dullemond & Dominik 2005).

6.3.1 MODELS Grain growth represents the baby steps toward planet formation. Over 13 orders of magnitude in linear size separate sub-micron particles from terrestrial planets, however, and many poorly understood processes operate along the way. Idealized dust coagulation models, ignoring fragmentation and radial drift, predict extremely efficient grain growth. Dullemond & Dominik (2005) investigated the dust coagulation process in circumstellar disks coupled to the settling and turbulent mixing of grains. They included 3 relatively well understood dust coagulation mechanisms (Brownian motion, differential settling and turbulence) and conclude that these processes are efficient enough to remove all small grains ($r < 100 \mu\text{m}$) within 10^4 yr . This is clearly inconsistent with the wealth of observational evidence showing the presence of micron sized grains throughout the duration of the primordial disk phase discussed in the next section. The conclusion is that small grains must be replenished and that the persistence of small grains depends on a complex balance between dust coagulation and fragmentation (Dullemond & Dominik 2008).

Recent, more realistic models including fragmentation and radial drift confirm the necessity of grain fragmentation to explain the ubiquity of small grains in disks (Birnstiel, Ormel & Dullemond 2011; Brauer, Dullemond & Henning 2008). These same models also confirm the severity of the problem known as the “meter-size barrier”, a physical scale at which solids are expected to suffer both destructive collisions and removal through rapid inward migration (Weidenschilling 1977). Even though several possible solutions have been proposed, including the formation of planetesimals in long-lived vortices (e.g., Heng & Kenyon 2010), or via the gravitational instability of millimeter-sized chondrules in a gas deficient subdisk (e.g., Youdin & Shu 2002), overcoming this barrier remains one of the biggest challenges for planet formation theories (Chiang & Youdin 2010).

6.3.2 EVIDENCE FOR GRAIN GROWTH FROM SUB-MICRON TO MICRONS Pristine dust in the interstellar medium is composed primarily of amorphous silicates,

generally olivine and pyroxene with characteristic features at 9.7 and 18.5 μm from Si–O stretching and O–Si–O bending modes, respectively. The shape of these features is a sensitive diagnostic of the size of small grains, generally in the $r \sim 0.1 - 5 \mu\text{m}$ range. Although the emission features of the smallest grains are strong and narrow, those of larger particles are weaker and broader. Thermal annealing can modify the lattice structure of magnesium-rich olivine and pyroxene and turn them into their crystallized forms, known as enstatite and forsterite (Henning 2010). These crystalline silicates have multi-peak features at slightly longer wavelengths than their amorphous counterparts.

Recent surveys with the IRS on *Spitzer* have allowed the study of silicates in hundreds of circumstellar disks in nearby star-forming regions (Furlan et al. 2006, 2009, Kessler-Silacci et al. 2006, McClure et al. 2010, Oliveira et al. 2010). Because these observations trace the warm optically thin disk “atmosphere”, and the larger particles are expected to settle toward the disk interior, they provide information on the smallest population of grains present in the disk. Nevertheless, the observed silicate features in most disks are consistent with the presence of micron-sized particles and the absence of sub-micron dust grains. This implies either that grain growth is more efficient than fragmentation at these scales or that sub-micron grains are efficiently removed from the upper layers of the disk by stellar winds or radiation pressure (Olofsson et al. 2009).

These *Spitzer* surveys have also shown that the signatures of grain growth and crystallization are seen at very early stages of disk evolution, even before the envelope has dissipated (Furlan et al. 2009, McClure et al. 2010). There seems to be little connection between the age or evolutionary stage of a primordial disk and the dust properties revealed by the silicate features. Even though many studies have searched for a correlation between the large scale properties of the disk (e.g., mass, accretion rates) and grain characteristics (sizes, degree of crystallization), no conclusive evidence has yet been found (e.g., Furlan et al. 2009, Kessler-Silacci et al. 2006, Oliveira et al. 2010). This lack of correlation between age and dust properties suggests that the characteristics of the dust population depend on a balance between grain growth and destruction and between crystallization (via thermal annealing) and amorphization (e.g., via X-ray irradiation, Glauser et al. 2009). This balance seems to persist throughout the duration of the primordial disk stage, at least in the surface layers of the disk.

6.3.3 EVIDENCE FOR GRAIN GROWTH FROM MICRONS TO MILLIMETERS A second, independent line of evidence for grain growth is found in the slope, α_{mm} , of the SED at sub-millimeter wavelengths, $F_\nu \propto \nu^{\alpha_{\text{mm}}}$. The slope between $\lambda \approx 0.5 - 1 \text{ mm}$ is significantly shallower in protoplanetary disks, $\alpha_{\text{mm}} \approx 2 - 3$ (Andrews & Williams 2005, 2007a, Beckwith & Sargent 1991, Mannings & Emerson 1994) than in the diffuse interstellar medium, $\alpha_{\text{mm}} \sim 4$ (Boulanger et al. 1996). In the Rayleigh-Jeans limit, the flux, $F_\nu \propto B_\nu(1 - e^{-\tau_\nu}) \rightarrow \nu^2$ for optically thick emission and $\rightarrow \kappa_\nu \nu^2$ for optically thin emission. The SED slope is therefore bound between $\alpha_{\text{mm}} = 2$ and $2 + \beta$ (see equation 2). Unresolved photometric observations include some optically thick emission from the inner disk so the connection between the observed disk average α_{mm} and the grain opacity index, β , requires modeling the surface density profile (Beckwith et al. 1990). For a simple power law thin disk model, Andrews & Williams (2005) show that $\alpha_{\text{mm}} - \beta$ lies between 1.1 and 1.8 for disk masses $10^{-2} - 10^{-5} M_\odot$ respectively, and is approximately independent of α_{mm} . Beckwith & Sargent (1991) and Mannings & Emerson

(1994) make similar corrections and all reach the same conclusion that the grain opacity index is significantly lower in disks, $\beta_{\text{disk}} \approx 0.5 - 1$, than in the interstellar medium, $\beta_{\text{ISM}} \approx 1.7$ (Li & Draine 2001).

The decrease in the dust opacity index is best explained by the presence of substantially larger dust grains in disks relative to the interstellar medium. For a power law distribution of grain sizes, $n(a) \propto a^{-p}$, D’Alessio, Calvet & Hartmann (2001) and Natta et al. (2004) show that $\beta \approx 1.7$ if the maximum grain size $a_{\text{max}} < 30 \mu\text{m}$ but then decreases to $\beta \lesssim 1$ for $a_{\text{max}} \gtrsim 0.5 \text{ mm}$ and $p = 2.5 - 3.5$. Draine (2006) provides a useful relation, $\beta \approx (p - 3)\beta_{\text{ISM}}$ if a_{max} is more than 3 times the observing wavelength, largely independent of grain composition. The implication of shallow disk SED slopes at sub-millimeter wavelengths relative to the diffuse interstellar medium is that dust grains have grown by at least 3 orders of magnitude, from microns to millimeters.

Some grain growth appears to happen in dense molecular cores before disks form. Growth to micron sizes is inferred from “coreshine”, or scattering, of mid-infrared light (Pagani et al. 2010). Shirley et al. (2000) measured the spectral slope for 21 cores, some pre-stellar, others in very early stages of low mass star formation and find an average spectral slope between 450 and 850 μm , $\alpha_{\text{mm}} = 2.8$, which is intermediate between the diffuse interstellar medium and protoplanetary disks. Multi-wavelength observations of Class 0 cores by Jørgensen et al. (2007) and Kwon et al. (2009) show opacity indices, $\beta \approx 1$, also shallower than the diffuse interstellar medium but not quite as steep as in protoplanetary disks.

There is also evidence that grain growth continues throughout the disk lifetime. Andrews & Williams (2005) find a significant difference in the SED slope between Taurus Class I (median $\alpha_{\text{mm}} = 2.5$) and Class II YSO disks (median $\alpha_{\text{mm}} = 1.8$). They also show that the sub-millimeter and infrared SED slopes are correlated with a best fit linear relationship, $\alpha_{\text{mm}} = 2.09 - 0.40\alpha_{\text{IR}}$. Confirmation of this single-dish result, which may be biased by cloud contamination in the early phases, requires interferometry.

These sub-millimeter data only place a lower bound on the size of the most massive grains. Longer wavelength observations constrain the presence of larger grains but the flux decreases (as the surface area of the dust decreases for a given mass) and the free-free emission from an ionized stellar wind often dominates for $\lambda \gtrsim 1 \text{ cm}$ (Natta et al. 2004). However, the correction for an opaque inner region is smaller. Surveys of Taurus disks have been carried out at 7 mm by Rodmann et al. (2006) and at 3 mm by Ricci et al. (2010b) who both find that the shallow SED slope generally extends to their observing wavelength and infer average opacity indices, $\langle\beta\rangle = 1, 0.6$ respectively. Similar results are found in other regions (Lommen et al. 2007, Ricci et al. 2011, 2010a). The implication is that centimeter sized particles are commonplace. The longest wavelength detection of dust in a protoplanetary disk to date was carried out by Wilner et al. (2005). By resolving the nearby, bright TW Hydra disk and showing that its flux is constant with time, they convincingly show that the 3.5 cm emission is from thermal dust emission and not accretion shocks or a stellar wind. The Draine (2006) formulation would therefore indicate the presence of $\sim 10 \text{ cm}$ sized bodies in the disk out at least to the 15 AU beam. A similar result has been found for WW Cha (Lommen et al. 2009).

Collisional grain growth (Blum & Wurm 2008) is expected to have a strong radial dependence due to the decreasing density and rotational velocity with increasing radius. Isella, Carpenter & Sargent (2010) resolve the RY Tau and DG

Tau disks at $\lambda = 1.3$ and 2.8 mm and model the data with a radially dependent dust opacity. However, to within their precision, $\Delta\beta = 0.7$, they do not see a significant gradient. We will soon see detailed images of β in disks and learn much more about the radial variation of grain growth via multi-wavelength observations with *ALMA*.

6.3.4 EVIDENCE FOR DUST SETTLING Protoplanetary disks are flared (see §4.3.2) and hence intercept and reprocess more stellar radiation than physically thin disks. Nevertheless, most T tauri stars exhibit less mid-infrared emission than expected for a disk in hydrostatic equilibrium. This can be understood in terms of dust settling which reduces the scale height and flaring angle of the disk (Dullemond & Dominik 2004). Mid-infrared slopes can therefore be used as a diagnostic of dust settling. D’Alessio et al. (2006) explored parametric models with two populations of grains: micron sized grains with a reduced dust-to-gas mass ratio in the surface layers of the disk, and mm-sized grains with an increased dust-to-gas mass ratio in the disk midplane. In order to quantify the degree of dust settling, they introduced the parameter ϵ , the ratio of the dust-to-gas mass ratio in the surface layer of the disk to the standard dust-to-gas mass ratio of the interstellar medium (1:100). In this context, $\epsilon = 1$ implies that no dust settling has occurred, and ϵ decreases as dust settling increases. D’Alessio et al. (2006) find that the median mid-infrared slopes of CTTS SEDs imply that $\epsilon \leq 0.1$ and possibly as low as 10^{-3} .

Furlan et al. (2006) applied these parametric models to reproduce the spectral slopes of a sample of over 80 Taurus T Tauri stars observed with the *Spitzer* Infrared Spectrograph. They conclude that most objects are consistent with dust depletion factors in the surface layers of the disk of order of 100 to 1000 (i.e., corresponding to $\epsilon = 10^{-2} - 10^{-3}$). A similar result is found by McClure et al. (2010) in the Ophiuchus molecular cloud. They also find evidence for significant dust settling in young (age ~ 0.3 Myr) objects embedded in the cloud core, suggesting that this process sets in early in the evolution of the disk (see also Furlan et al. 2009).

6.4 Typical evolution and diversity of evolutionary paths

Although we are far from fully understanding the complex evolution of protoplanetary disks, a coherent picture is starting to emerge from the many models and observational constraints discussed above. Although it is clear that not all disks follow the same evolutionary path, many observational trends suggest that most objects do follow a common sequence of events. In what follows we summarize our current understanding of the “typical” evolution of a protoplanetary disk.

6.4.1 THE EVOLUTION OF A TYPICAL DISK Early in its evolution, the disk loses mass through accretion onto the star and FUV photoevaporation of the outer disk (Gorti, Dullemond & Hollenbach 2009). The FUV photoevaporation is likely to truncate the outer edge of the disk, limiting its viscous expansion to a finite size of several hundreds of AU in diameter (Figure 6a). During this “mass depletion” stage, which can last several Myr, an object would be classified as a CTTS based on the presence of accretion indicators. Accretion may be variable on short timescales, but show a declining long-term trend.

At the same time, grains grow into larger bodies that settle onto the mid-plane of the disk where they can grow into rocks, planetesimals and beyond. Accord-

ingly, the scale height of the dust decreases and the initially-flared dusty disk becomes flatter (Figure 6b). This steepens the slope of the mid and far-infrared SED as a smaller fraction of the stellar radiation is intercepted by circumstellar dust (Dullemond & Dominik 2005). The near-infrared fluxes remain mostly unchanged because the inner disk stays optically thick and extends inward to the dust sublimation temperature. The most noticeable SED change during this stage is seen in the decline of the (sub-)millimeter flux, which traces the decrease in the mass of millimeter and smaller sized particles (Andrews & Williams 2005, 2007a, Figure 7).

As disk mass and accretion rate decrease, energetic photons from the stellar chromosphere are able to penetrate the inner disk and photoevaporation becomes important. When the accretion rate drops to the photoevaporation rate, the outer disk is no longer able to resupply the inner disk with material (Alexander, Clarke & Pringle 2006a; Owen et al. 2010). At this point, the inner disk drains on a viscous timescale ($\lesssim 10^5$ yr) and an inner hole of a few AU in radius is formed in the disk (Figure 6c). Once this inner hole has formed, the energetic photons impact the inner edge of the disk unimpeded, and the photoevaporation rate increases further, preventing any material from the outer disk from flowing into the inner hole. This halts accretion and results in the rapid transition between the CTTS and the WTTS stage.

The formation of the inner hole marks the end of the slow “mass depletion” phase and the beginning of the of the rapid “disk dissipation” stage. By the time the inner hole is formed, the mass of the outer disk is believed to be $\lesssim 1-2 M_{\text{Jup}}$, as attested by the low mass of WTTS disks (Andrews & Williams 2005, 2007a, Cieza et al. 2010, 2008). During this “disk dissipation” stage, the SEDs of the WTTS disks present a wide range of morphologies, as expected for disks with inner holes of different sizes (Cieza et al. 2007, Padgett et al. 2006, Wahhaj et al. 2010). Once the remaining gas photoevaporates, the dynamics of the solid particles become dominated by radiation effects (Figure 6d). Although the small ($r \lesssim 1 \mu\text{m}$) grains are quickly blown out by radiation pressure, slightly larger ones spiral in due to the Poynting-Robertson effect and eventually evaporate when they reach the dust sublimation radius. What is left represents the initial conditions of a debris disk: a gas poor disk with large grains, planetesimals and/or planets. The fact that the vast majority of WTTS show no evidence for a disk (primordial or debris) implies that not every primordial disk evolves into a detectable debris disks. Whether some disks remain detectable throughout the primordial to debris disk transition or there is always a quiescent period between these two stages still remains to be established.

6.4.2 THE AGE VARIABLE Although it is true that there is some discernible correlation between the ages of pre-main sequence stars and the evolutionary stages of their disks, this correlation is rather weak. In fact, circumstellar disks in every stage of evolution, from massive primordial disks to debris disks and completely dissipated disks, are seen in stellar clusters and associations with ages ranging from $\lesssim 1$ Myr to ~ 10 Myr (e.g., Muzerolle et al. 2010). Diskless WTTS in the core of the young Ophiuchus molecular cloud and the relatively old, gas-rich TW Hydra are good examples of these extremes. This weak correlation between stellar age and disk evolutionary stage can be explained by the combination of two factors: the wide range in the duration of the “mass depletion” stage and the short time scale of the “disk dissipation” phase. On the one hand, as discussed

in §5.6.1, circumprimary disks in medium separation binary systems are likely to have truncated disks with small initial masses. Because the “mass depletion” stage in such objects is expected to be very short ($\lesssim 0.3$ Myr), their circumstellar disks can easily go through all the evolutionary stages described above in less than 1 Myr. However, initially massive circumstellar disks evolving in isolation can in principle remain optically thick at all infrared wavelengths for up to ~ 10 Myr.

6.4.3 EVIDENCE FOR ALTERNATIVE EVOLUTIONARY PATHS The observed properties of most circumstellar disks are consistent with the evolutionary sequence shown in Figure 6; however, some outliers do exist, showing that not all disks follow the same sequence of event in an orderly manner. Perhaps the most intriguing outliers are accreting objects that have cleared out inner disks but retained massive ($> 10 M_{\text{Jup}}$) outer disks. Examples of such objects, which represent a small subgroup of the so-called transition disks, include DM Tau, GM Aur (Najita, Strom & Muzerolle 2007), and RX J1633.9-2442 (Cieza et al. 2010). Their large accretion rates, inner radii, and disk masses make their holes incompatible with the evolutionary sequence discussed above. We must then consider an additional agent, most likely dynamical clearing by a (sub)stellar or planetary-mass companion. The nature of these objects is discussed in some detail in the following section.

6.5 Section summary

- Protoplanetary disks evolve through a variety of processes, including viscous transport, photoevaporation from the central star, grain growth and dust settling, and dynamical interaction with (sub)stellar and planetary-mass companions.
- Photoevaporative flows from disk surfaces have been observed but the models disagree on the relative importance of FUV, EUV, and X-ray photoevaporation.
- There is strong evidence for grain growth to millimeter (and, in some cases, centimeter) sizes but the presence and distribution of larger bodies remain unconstrained.
- Most protostellar disks go through a slow “mass depletion” phase followed by a rapid “disk dissipation” stage. As the accretion rate steadily drops below the photoevaporative rate, the disk is rapidly eroded from the inside-out. A wide range in the duration of the two phases, together with the intrinsic dispersion of disk masses and radii, weakens the correlation between stellar age and disk evolutionary stage.

7 TRANSITION DISKS

Transition disks were first identified by *IRAS* as objects with little or no excess emission at $\lambda < 10 \mu\text{m}$ and a significant excess at $\lambda \geq 10 \mu\text{m}$ (Strom et al. 1989, Wolk & Walter 1996). The lack of near-infrared excess was interpreted as a diagnostic of inner disk clearing possibly connected to the early stages of planet formation. Because of this possible connection, transition disks have received special attention in circumstellar disks studies even though they represent a small percentage of the disk population in nearby star-forming regions. In this section we discuss the diversity of SED morphologies presented by transition disks, their

incidence, and their connection to planet formation and other disk evolution processes.

7.1 SED diversity and interpretation

Transition disks present a variety of infrared SED morphologies and their diversity is not properly captured by the traditional classification scheme of young stellar objects (i.e., the Class I through III system, see § 2). In order to better describe the shape of transition disk SEDs, Cieza et al. (2007) introduced a two-parameter scheme based on the longest wavelength at which the observed flux is dominated by the stellar photosphere, $\lambda_{\text{turn-off}}$, and the slope of the infrared excess, α_{excess} , computed from $\lambda_{\text{turn-off}}$ to $24\,\mu\text{m}$ (Figure 8a.)

Because of their diversity, the precise definition of what constitutes a transition object found in the disk-evolution literature is far from homogeneous. Transition disks have been defined as objects with no detectable near-infrared excess, steep slopes in the mid-infrared, and large far-infrared excesses (Muzerolle et al. 2010, Sicilia-Aguilar, Henning & Hartmann 2010). This definition is the most restrictive one and effectively corresponds to objects with $\lambda_{\text{turn-off}} \gtrsim 4.5 - 8.0\,\mu\text{m}$ and $\alpha_{\text{excess}} > 0$. The above definition has been relaxed by some researchers (Brown et al. 2007; Merin et al. 2010) to include objects with small, but still detectable, near-infrared excesses. Transition disks have also been more broadly defined in terms of a significant decrement relative to the median SED of CTTS at any or all infrared wavelengths (Cieza et al. 2010; Najita, Strom & Muzerolle 2007). Several nouns have recently emerged in the literature to distinct sub-classes of transition disks (Evans et al. 2009a). Objects with no detectable near-infrared excess and $\alpha_{\text{excess}} > 0$ have been called “classical” transition disks (Muzerolle et al. 2010), whereas other objects with a sharp rise in their mid-infrared SEDs have been termed “cold disks” (Brown et al. 2007, Merin et al. 2010) regardless of the presence of near-infrared excess. Disks with a significant flux decrement at all infrared wavelengths relative to the SED of an optically thick disk extending to the dust sublimation temperature typically have $\alpha_{\text{excess}} < 0$ and been referred to as “anemic” disks (Lada et al. 2006), “homologously depleted” disks (Currie et al. 2009), or “weak excess” disks (Muzerolle et al. 2010). Finally, disks with evidence for an optically thin (to starlight) gap separating optically thick inner and outer disk components have been called “pre-transition” disks (Espaillat et al. 2007, 2010) because they are believed to be precursors of objects with sharp, but empty inner holes (i.e., the “classical” transition disks mentioned above).

The inherent diversity of transition disk SEDs is encapsulated in Figure 8b which shows how the range of slopes, α_{excess} , increases as the point at which excess emission is detected, $\lambda_{\text{turn-off}}$, increases. Disks without inner holes, $\lambda_{\text{turn-off}} \lesssim 2\,\mu\text{m}$, have similar mid-infrared SED slopes but this is not the case for larger $\lambda_{\text{turn-off}}$ suggesting a range of processes by which the inner hole is formed and develops.

Examples of the different types of transition disk SEDs are shown in Figure 9. The SEDs that decrease in the mid-infrared, $\alpha_{\text{excess}} \lesssim 0$, have generally been interpreted as evidence for grain growth and dust settling toward the midplane (Cieza et al. 2010, Lada et al. 2006, Sicilia-Aguilar, Henning & Hartmann 2010). Both processes tend to reduce the mid-infrared fluxes. Grain growth removes small grains and thus reduces the opacity of the inner disk. Dust settling results in flatter disks that intercept and reprocess a smaller fraction of the stellar radiation. This group of objects includes anemic, homologously depleted disks,

and weak-excess disks. Objects with rising mid-infrared SEDs, $\alpha_{\text{excess}} > 0$, a group that includes classical transition disks, cold disks, and pre-transition disks, are more consistent with a steep radial dependence in the dust opacity resulting in a sharp boundary to the inner opacity hole. These may be due to dynamical clearing by a companion, possibly planetary (Artymowicz & Lubow 1994), or photoevaporation (Alexander, Clarke & Pringle 2006b). Debris disks also have sharp inner holes but they can be distinguished by their low luminosities and lack of gas.

7.2 Incidence

Establishing the incidence of transition disks is not straightforward given the different definitions used by different studies. Also, samples are usually not complete and thus suffer from selection effects. Furthermore, several background objects can mimic the SEDs of some types of transition disks and skew the statistics. In particular, Asymptotic Giant Branch stars and classical Be stars can be easily confused with “weak excess” transition disks (Cieza et al. 2010, Oliveira et al. 2010), and the SEDs of edge-on protoplanetary disks can look like those of cold disks (Merín et al. 2010).

With these caveats, the fraction of disks in nearby star-forming regions that are seen in a transition stage is thought to be $\lesssim 10 - 20\%$ (Currie et al. 2009, Dahm & Carpenter 2009, Fang et al. 2009, Hernández et al. 2007, Kim et al. 2009, Lada et al. 2006). Also, it is clear that “weak-excess” (or “anemic” and “homologously depleted”) transition disks outnumber, by factors of $\sim 2 - 3$, objects with sharp inner holes (Cieza et al. 2010, Muzerolle et al. 2010). The fraction of cold disks in nearby star-forming regions has been recently established to lie between 5 and 10% (Merín et al. 2010, Oliveira et al. 2010).

Weak-excess disks seem to be more common in older clusters (Muzerolle et al. 2010). This is expected because disks should become flatter and lose mass with time (see §6.4). Weak-excess disks appear to be much more abundant around young (age ~ 1 Myr) M-stars than around solar-type stars of the same age (Sicilia-Aguilar et al. 2008). However, this may be a luminosity effect rather than an evolutionary one. Because M-type stars are much fainter and cooler than solar-type stars, they may present weak mid-infrared excess emission even if the disk extends in to the dust sublimation radius (Ercolano, Clarke & Robitaille 2009).

The relatively small number of objects seen in a transition stage suggests that the evolutionary path through a transitional disk is either uncommon or rapid. However, observations show that an infrared excess at a given wavelength is always accompanied by a larger excess at longer wavelengths, out to $\sim 100 \mu\text{m}$. This implies that, unless some disks manage to lose the near-, mid-, and far-infrared excess at exactly the same time, the near-infrared excess always dissipates before the mid-infrared and far-infrared excess do. No known process can remove the circumstellar dust at all radii simultaneously, and even if grain growth or dynamical clearing do not produce an inner hole, photoevaporation by the central star will do so once the accretion rate through the disk falls below the photoevaporation rate. Therefore, it is reasonable to conclude that transition disks represent a common but relatively short phase in the evolution of a circumstellar disk. Of course, how long the transition stage lasts for a given disk strongly depends on the nature of each object. On the one hand, the transition phase should be very

short, < 0.5 Myr, if the inner hole is formed through photoevaporation. However, an object could in principle show a transition disk SED for a longer period of time if the inner opacity hole is due to grain growth, or giant planet formation.

7.3 Physical properties

Although it is clear that many different processes can result in transition disk SEDs, the relative importance of these processes is not well understood. Distinguishing among processes requires additional observational constraints on the physical properties of these objects, such as disk mass, accretion rates, fractional disk luminosities ($L_{\text{disk}}/L_{\text{star}}$), and multiplicity information. These observational constraints have only recently been obtained for statistically significant samples of transition disks.

Najita, Strom & Muzerolle (2007) investigated the SEDs, disk masses, and accretion rates of over 60 Taurus pre-main sequence stars and identified 12 transition disks. Based on their SEDs, 7 of these 12 could be further classified as weak excess disks, 3 as classical transition disks, and 2 as pre-transition disks. They found that the transition disks in their sample have larger average disk masses and lower average accretion rates than non-transition disks around single stars. They concluded that, with the exception of CoKu Tau 4, the SEDs were all more consistent with the giant planet formation scenario than with photoevaporation models (which at the time predicted negligible accretion rates and lower disk masses) and grain growth (which would favor higher accretion rates for a given disk mass). However, because their sample was drawn from the *Spitzer* spectroscopic survey of Taurus presented by Furlan et al. (2006), who in turn selected their targets based on mid-infrared colors from *IRAS*, their sample was biased towards the brightest objects in the mid-infrared and are unlikely to represent the overall population of transition disks.

As a counter example, Cieza et al. (2008) studied over 20 WTTS with transition disk SEDs, found that all had very small disk masses ($\lesssim 2 M_{\text{Jup}}$), and concluded they were all consistent with the EUV photoevaporation models of Alexander, Clarke & Pringle (2006a,b). Sicilia-Aguilar, Henning & Hartmann (2010) studied accretion rates in a sample of 95 members of the ~ 4 Myr Tr 37 cluster. They found that half of the 20 classical transition disks in their sample had evidence for accretion (i.e. their holes contain gas but no dust) and half were non-accreting (i.e., their holes are really empty). Furthermore, the accretors had rates that were indistinguishable from those of regular CTTS in the cluster, a result that is at odds with the Taurus sample studied by Najita, Strom & Muzerolle (2007). These discrepancies show that transition disks are a highly heterogeneous group of objects and that the mean properties of a given sample are highly dependent on the details of the sample selection criteria and, thus, should be interpreted with caution.

Cieza et al. (2010) studied a sample of 26 transition disks in Ophiuchus. With the exception of edge-on disks, highly embedded objects, and the lowest mass transition objects, all of which are too faint in the optical to pass one of their selection criteria, the sample is likely to be representative of the entire transition disk population in the Ophiuchus molecular cloud. They find that 9 of the 26 targets have low disk masses ($< 2.5 M_{\text{Jup}}$) and negligible accretion, and are thus consistent with photoevaporation. 4 of these 9 non-accreting objects have fractional disk luminosities $< 10^{-3}$, however, and could already be in a debris

disk stage. The other 17 objects in the sample are accreting. 13 of these are consistent with dust settling and grain growth ($\alpha_{\text{excess}} \lesssim 0$), whereas the other 4 have rising mid-infrared SEDs ($\alpha_{\text{excess}} > 0$) indicative of sharp inner holes, and are candidates for harboring embedded giant planets. A decision tree showing the different possibilities is shown in Figure 10.

Interestingly, non-accreting objects with relatively massive disks ($\gtrsim 2.5 M_{\text{Jup}}$) are absent in the Ophiuchus transition disk sample. Such objects are rare but do exist. The “cold disk” around T Cha is an example (Brown et al. 2007), and its properties could be explained by a companion massive enough to disrupt accretion onto the star. A few accreting binary systems are known, however, for example, DQ Tau (Carr, Mathieu & Najita 2001) and CS Cha (Espaillat et al. 2007), which implies that a massive companion does not always stop accretion. The eccentricity of the orbit, and the viscosity and scale height of the disk also determine whether accretion onto the star can continue (Artymowicz & Lubow 1996).

Binarity is also known to result in transition disk SEDs. Identifying close companions is particularly difficult, however, especially if they are within the inner $\sim 5 - 10$ AU of the disk, which is beyond the near-infrared diffraction limit of $8 - 10$ m class telescopes at the distance of the nearest star-forming regions ($\sim 125 - 140$ pc). Using the aperture masking technique in a single Keck telescope, Ireland & Kraus (2008) showed that CoKu Tau 4 is a near-equal mass binary system, which explains the inner hole that had been inferred from its SED; nevertheless, it is clear that not all sharp inner holes are due to binarity. DM Tau, GM Aur, LkCa 15, UX Tau, and RY Tau have all been observed with the Keck interferometer (Pott et al. 2010). For these objects, all of which show evidence for accretion unlike CoKu Tau 4, stellar companions with flux ratios $\lesssim 20$ can be ruled out down to sub-AU separations.

7.4 Resolved observations

Although SED modeling provides strong evidence for the presence of inner holes in some transition disks, this evidence is indirect and model-dependent. Long baseline interferometry at (sub-)millimeter wavelengths, however, can directly image the inner holes of some transition disks in nearby star-forming regions.

Inner holes have finally been resolved in a number of transition disks in recent years. Figure 11 displays a montage of images at the same linear scale in comparison to the orbits of the giant planets in the Solar System. The holes can be clearly seen in the face-on disks and are apparent through a central dip in the emission for edge-on disks.

Because the emission is optically thin in these (sub-)millimeter data, the images directly show the mass surface density profile of the disk and can be used to measure the size and sharpness of inner holes. In most cases, the (sub-)millimeter interferometry confirms the expected sizes of the inner holes (ranging from ~ 4 AU to ~ 50 AU in radius) and their sharpness (i.e., a large increase in the dust density over a small range in radii) predicted from the SED. For example, Brown et al. (2009) and Andrews et al. (2010b) show that the flux decrement toward the centers of their imaged transition disks are consistent with step functions with dust depletion factors ranging from 10^2 to 10^4 .

Several of these transition disks are gas rich. In two cases, GM Aur and J1604-2130, where the millimeter CO emission is resolved to sufficient detail either

spectroscopically or spatially, the central cavity is found to be not only dust but also gas deficient (Dutrey et al. 2008, respectively). However, Pontoppidan et al. (2008) found mid-infrared CO emission from well inside the dust gaps in SR 21, HD 135344, and TW Hya.

The details in millimeter interferometric images may contain dynamical hints of giant planets. All the images in Figure 11 appear to be asymmetric but these are no more than suggestions given the modest signal-to-noise ratio and poor sampling of the Fourier plane. Hughes et al. (2009a) note a warp between the dust and gas structures in GM Aur. High fidelity images with *ALMA* will soon allow us to study the structure of circumstellar disks in much greater detail, and the incidence of radial gaps, density waves, warps, and other possible azimuthal asymmetries should become evident. It may well be possible to find earlier stages in the disk clearing process through a decline in the millimeter flux before the infrared opacity drops below unity (Andrews et al. 2008).

In addition to the (sub-)millimeter images discussed above, in at least one case, LkCa 15, the inner hole has been imaged in the near-infrared from starlight reflected from the edge of a disk wall ~ 50 AU in radius (Thalmann et al. 2010) once again confirming the structure inferred from modeling the SED of the object.

7.5 Section summary

- Transition disks can be broadly defined as disks with a significant flux decrement relative to the median SED of CTTS at any or all infrared wavelengths. They constitute at most 20% of the disk population.
- There is a wide range of transition disk SEDs, indicative of the varied physical processes, photoevaporation, grain growth, and dynamical interactions with companions or planets, that produce them.
- Grain growth and dust settling produce SEDs with falling mid-infrared emission ($\alpha_{\text{excess}} \lesssim 0$). SEDs that rise in the mid-infrared ($\alpha_{\text{excess}} > 0$) are more consistent with a sharp boundary to the inner hole due to photoevaporation or dynamical interactions.
- Giant planet formation best explains the combination of accretion and steeply rising mid-infrared emission in moderately massive disks, $M \gtrsim 3 M_{\text{Jup}}$.

8 SUMMARY POINTS

Observations of protoplanetary disks are challenging due to their small size, low masses, and cool temperatures. However a number of basic facts have been clearly established. Mid-infrared observations of optically thick emission provide the most sensitive measures of the presence of a disk through which we infer their occurrence and lifetimes. Millimeter wavelength observations of optically thin emission provide the best measures of disk masses and, through interferometry, resolved images of their structure. The interpretation of the data is complicated by the uncertainties in our knowledge of grain growth and settling, gas dispersal, and the feedback between composition and structure. Nevertheless, it is clear that there are a variety of evolutionary pathways, and many different physical processes competing with each other, including planet formation. Even the restricted subject area of this review on observations of the outer disk is so large

that we have given a summary to each section. Here, we distill these summaries yet further into six main points.

- Circumstellar disks form almost immediately after a molecular core collapses. They appear to be highly unstable at early times and accrete in bursts onto the central protostar.
- By the time a YSO becomes optically visible, the mass of the now protoplanetary disk averages 1% that of the central star. Its surface density increases approximately inversely with radius and it has a soft, exponentially tapered edge between a few tens to hundreds of AU. The disks are now generally stable and rotate with a Keplerian velocity profile. About 15% of disks around solar mass stars have a MMSN ($10 M_{\text{Jup}}$) of material within 50 AU radius.
- Disks around solar and lower mass stars have a median lifetime between 2 and 3 Myr but with a large dispersion from less than 1 Myr to a maximum of 10 Myr. Lifetimes are shorter around higher mass stars and binaries with semi-major axes between 5 and 100 AU. The large scale environment is relatively unimportant: disruption by stellar flybys is very rare and photoevaporation by massive stars generally only erodes the outer disk, beyond about 50 AU.
- Protoplanetary disks evolve through a variety of processes, including viscous transport, photoevaporation by the central star, grain growth and dust settling, and dynamical interaction with (sub)stellar and planetary-mass companions. Most disks evolve via a slow decrease in the mass of gas and small particles followed by rapid disk clearing at all radii.
- The growth of dust grains from sub-micron sizes in the ISM to millimeter sizes in disks occurs early and continues with time. The presence of snowballs or pebbles several centimeters in size is hard to measure but has been inferred in a couple of cases.
- About 10-20% of disks show mid-infrared dips indicative of inner holes. They present a wide range of SED morphologies and physical properties (disk masses, accretion rates, and inner hole sizes). These transition disks are excellent laboratories to study the disk clearing phase and the formation of planets.

9 FUTURE ISSUES

Protoplanetary disks emit predominantly at long wavelengths where the atmospheric background is high, and where high resolution requires interferometry. By necessity, many current observations are of the brightest disks but these may not be truly representative. Systematic studies of the median disk population are about to become routine. Ongoing observations with *Herschel* at far-infrared wavelengths around the peak of their SED are just beginning to produce new insights into disk structure, chemistry, and evolution. Within the next few years, *ALMA* will dramatically expand upon the pathfinder work of present-day interferometers at (sub-)millimeter wavelengths. Further down the line lies the prospect of sensitive, high resolution observations in the mid-infrared with thirty-meter class telescopes, as well as at centimeter and longer wavelengths with the Square

Kilometer Array. There is an enormous range of issues to investigate with these and other instruments. Here, we list those that we find particularly compelling.

- *Disk formation:* With the high sensitivity and imaging fidelity of *ALMA*, it will be possible to map faint isotopic lines of dense gas tracers and search for small rotationally supported structures in the centers of molecular cores. Instabilities may be revealed through spiral waves and other asymmetries and can provide an independent dynamical disk mass estimate. Optically thick lines seen in absorption against the disk continuum will show the infall of material from the core. Multi-wavelength continuum imaging will track the increase in the grain size distribution through the process.
- *Peering into the terrestrial planet zone:* Very high resolution observations, $\lesssim 0''.1$, at wavelengths beyond a millimeter can image optically thin dust emission and resolve structures in the terrestrial planet-forming zone, $R \lesssim 5$ AU, of the closest disks. The longer the wavelength of the observation, the larger the size of the dust grains that can be detected. The first systematic studies at centimeter wavelengths are just beginning with the extended *VLA*. The Square Kilometer Array will measure the distribution of rocks and snowballs up to meter sizes. Together with *ALMA*, resolved images from sub-millimeter to centimeter wavelengths will show the radial variation of grain growth.
- *Disk chemistry:* The ability to survey many disks in many lines with *ALMA* will revolutionize the young field of disk chemistry. As different species and transitions are excited in different regions of a disk, such observations will enable a far more complete picture of the gas disk structure to be developed. Observations of H_2^{18}O will reveal the water context of disks and constrain the location of the snowline in a statistically meaningful sample. The detection of other molecular isotopologues will allow isotopic abundances (and radial gradients) to be measured and directly compared to cosmochemical studies of meteorites.
- *What is the overall evolution of the gas-to-dust mass ratio in circumstellar disks?* Although the evolution of the dust ($r \lesssim 1$ mm) content in disks can be traced reasonably well by current (sub)millimeter observations, our current understanding of the evolution of the gas is very limited. Observations of gas tracers with *Herschel* (e.g., [O I] at $63.2 \mu\text{m}$), large infrared telescopes (e.g., H_2 at 12.4 and $17.0 \mu\text{m}$), and *ALMA* (e.g., rotational lines of CO and its isotopologues) will reveal the evolution of the gas and the gas-to-dust ratio, which is critical to understanding the formation of both terrestrial and giant planets.
- *How and when do giant planets form?* Although much progress has been made in understanding the structure and evolution of circumstellar disks, this fundamental question still remains unanswered. Detailed studies of embedded (Class I) disks with *ALMA* will help to establish whether massive young disks can be conducive to the formation of giant planets through gravitational instability. Similarly, planet searches in Class II YSOs, and transition disks in particular, with thirty-meter class infrared telescopes will identify young giant planets at the last stages of the core accretion process.
- *Toward comprehensive disk evolution models:* To date most disk evolution models have focused on one or two physical processes at a time (e.g., viscous

accretion and photoevaporation) while ignoring other equally important ones (e.g., grain growth and dust settling and dynamical interactions with (sub)stellar companions and/or young planets). In reality, however, it is clear that all these processes are likely to operate simultaneously and affect one another, and that any realistic disk evolution model should include all known disk evolution mechanisms.

- *Placing our Solar System in context:* The small number of protoplanetary disks that have been studied in detail each have their own idiosyncracies. Whereas there are rough matches to the mass, size, and surface density profile of the MMSN, it is not clear how common these conditions were. Improvements in technology at all wavelengths will allow more refined studies of the closest disks and large surveys of more distant star-forming regions. In tandem with the ever increasing knowledge-base on the number, mass, and density distribution of exoplanets, we will gather the detailed statistics necessary to understand what is typical and what is atypical about the protosolar nebula.

10 Acknowledgements

We gratefully acknowledge Ewine van Dishoeck, Michiel Hogerheijde and Neal Evans for their detailed comments. We also thank Sean Andrews, Joanna Brown, Stephane Guilloteau, Paul Harvey, Meredith Hughes, Andrea Isella, Antonella Natta, Ilaria Pascucci, Charlie Qi, and Goran Sandell for reading an early version of this manuscript, assistance with figures, or sharing data. This work is funded through grants from the National Science Foundation and the National Aeronautics and Space Administration through the *Spitzer* and *Sagan* Fellowship programs.

References

- Acke B, van den Ancker ME, Dullemond CP. 2005. *A&A* 436:209–230
- Acke B, van den Ancker ME, Dullemond CP, van Boekel R, Waters LBFM. 2004. *A&A* 422:621–626
- Adams FC, Hollenbach D, Laughlin G, Gorti U. 2004. *Ap. J.* 611:360–379
- Adams FC, Lada CJ, Shu FH. 1987. *Ap. J.* 312:788–806
- Alexander RD, Clarke CJ, Pringle JE. 2006a. *MNRAS* 369:216–228
- Alexander RD, Clarke CJ, Pringle JE. 2006b. *MNRAS* 369:229–239
- Alonso-Albi T, Fuente A, Bachiller R, Neri R, Planesas P, et al. 2009. *A&A* 497:117–136
- André P, Montmerle T. 1994. *Ap. J.* 420:837–862
- André P, Ward-Thompson D, Barsony M. 1993. *Ap. J.* 406:122–141
- Andrews SM, Czekala I, Wilner DJ, Espaillat C, Dullemond CP, Hughes AM. 2010a. *Ap. J.* 710:462–469
- Andrews SM, Hughes AM, Wilner DJ, Qi C. 2008. *Ap. J. Lett.* 678:L133–L136
- Andrews SM, Williams JP. 2005. *Ap. J.* 631:1134–1160
- Andrews SM, Williams JP. 2007a. *Ap. J.* 671:1800–1812

- Andrews SM, Williams JP. 2007b. *Ap. J.* 659:705–728
- Andrews SM, Wilner DJ, Hughes AM, Qi C, Dullemond CP. 2009. *Ap. J.* 700:1502–1523
- Andrews SM, Wilner DJ, Hughes AM, Qi C, Dullemond CP. 2010b. *Ap. J.* 723:1241–1254
- Armitage PJ. 2010. *ArXiv e-prints*
- Artymowicz P, Lubow SH. 1994. *Ap. J.* 421:651–667
- Artymowicz P, Lubow SH. 1996. *Ap. J. Lett.* 467:L77+
- Bally J, O’Dell CR, McCaughrean MJ. 2000. *A. J.* 119:2919–2959
- Balog Z, Muzerolle J, Rieke GH, Su KYL, Young ET, Megeath ST. 2007. *Ap. J.* 660:1532–1540
- Balog Z, Rieke GH, Muzerolle J, Bally J, Su KYL, et al. 2008. *Ap. J.* 688:408–417
- Balog Z, Rieke GH, Su KYL, Muzerolle J, Young ET. 2006. *Ap. J. Lett.* 650:L83–L86
- Barrado y Navascués D, Martín EL. 2003. *A. J.* 126:2997–3006
- Basu S. 1998. *Ap. J.* 509:229–237
- Beckwith SVW, Sargent AI. 1991. *Ap. J.* 381:250–258
- Beckwith SVW, Sargent AI. 1996. *Nature* 383:139–144
- Beckwith SVW, Sargent AI, Chini RS, Guesten R. 1990. *A. J.* 99:924–945
- Bergin EA. 2009. *ArXiv e-prints*
- Bergin EA, Hogerheijde MR, Brinch C, Fogel J, Yıldız UA, et al. 2010. *A&A* 521:L33+
- Bergin EA, Tafalla M. 2007. *Ann. Rev. Astron. Astrophys.* 45:339–396
- Beust H, Dutrey A. 2005. *A&A* 439:585–594
- Birnstiel T, Ormel CW, Dullemond CP. 2011. *A&A* 525:A11+
- Bitner MA, Richter MJ, Lacy JH, Greathouse TK, Jaffe DT, Blake GA. 2007. *Ap. J. Lett.* 661:L69–L72
- Bitner MA, Richter MJ, Lacy JH, Herczeg GJ, Greathouse TK, et al. 2008. *Ap. J.* 688:1326–1344
- Black DC, Matthews MS, eds. 1985. *Protostars and planets II*
- Blum J, Wurm G. 2008. *Ann. Rev. Astron. Astrophys.* 46:21–56
- Boulanger F, Abergel A, Bernard J, Burton WB, Desert F, et al. 1996. *A&A* 312:256–262
- Brauer F, Dullemond CP, Henning T. 2008. *A&A* 480:859–877
- Brinch C, Crapsi A, Jørgensen JK, Hogerheijde MR, Hill T. 2007. *A&A* 475:915–923
- Brown DW, Chandler CJ, Carlstrom JE, Hills RE, Lay OP, et al. 2000. *MNRAS* 319:154–162
- Brown JM, Blake GA, Dullemond CP, Merín B, Augereau JC, et al. 2007. *Ap. J. Lett.* 664:L107–L110

- Brown JM, Blake GA, Qi C, Dullemond CP, Wilner DJ, Williams JP. 2009. *Ap. J.* 704:496–502
- Burrows CJ, Stapelfeldt KR, Watson AM, Krist JE, Ballester GE, et al. 1996. *Ap. J.* 473:437–+
- Calvet N, Briceño C, Hernández J, Hoyer S, Hartmann L, et al. 2005. *A. J.* 129:935–946
- Carmona A, van den Ancker ME, Henning T, Pavlyuchenkov Y, Dullemond CP, et al. 2008. *A&A* 477:839–852
- Carpenter JM, Bouwman J, Mamajek EE, Meyer MR, Hillenbrand LA, et al. 2009. *Ap. J. Suppl.* 181:197–226
- Carpenter JM, Mamajek EE, Hillenbrand LA, Meyer MR. 2006. *Ap. J. Lett.* 651:L49–L52
- Carr JS, Mathieu RD, Najita JR. 2001. *Ap. J.* 551:454–460
- Carr JS, Najita JR. 2008. *Science* 319:1504–
- Caselli P, Walmsley CM, Tafalla M, Dore L, Myers PC. 1999. *Ap. J. Lett.* 523:L165–L169
- Ceccarelli C, Dominik C, Lefloch B, Caselli P, Caux E. 2004. *Ap. J. Lett.* 607:L51–L54
- Chandler CJ, Brogan CL, Shirley YL, Loinard L. 2005. *Ap. J.* 632:371–396
- Chapillon E, Parise B, Guilloteau S, Dutrey A, Wakelam V. 2010. *A&A* 520:A61+
- Chiang E, Kite E, Kalas P, Graham JR, Clampin M. 2009. *Ap. J.* 693:734–749
- Chiang E, Youdin AN. 2010. *Annual Review of Earth and Planetary Sciences* 38:493–522
- Chiang EI, Goldreich P. 1997. *Ap. J.* 490:368–+
- Chiang EI, Joungh MK, Creech-Eakman MJ, Qi C, Kessler JE, et al. 2001. *Ap. J.* 547:1077–1089
- Chiang H, Looney LW, Tassis K, Mundy LG, Mouschovias TC. 2008. *Ap. J.* 680:474–482
- Ciesla FJ, Cuzzi JN. 2006. *Icarus* 181:178–204
- Cieza L, Padgett DL, Stapelfeldt KR, Augereau J, Harvey P, et al. 2007. *Ap. J.* 667:308–328
- Cieza LA, Padgett DL, Allen LE, McCabe CE, Brooke TY, et al. 2009. *Ap. J. Lett.* 696:L84–L88
- Cieza LA, Schreiber MR, Romero GA, Mora MD, Merin B, et al. 2010. *Ap. J.* 712:925–941
- Cieza LA, Swift JJ, Mathews GS, Williams JP. 2008. *Ap. J. Lett.* 686:L115–L118
- Clarke CJ. 2007. *MNRAS* 376:1350–1356
- Clarke CJ, Gendrin A, Sotomayor M. 2001. *MNRAS* 328:485–491
- Corder S, Eisner J, Sargent A. 2005. *Ap. J. Lett.* 622:L133–L136
- Crutcher RM, Hakobian N, Troland TH. 2009. *Ap. J.* 692:844–855
- Currie T, Lada CJ, Plavchan P, Robitaille TP, Irwin J, Kenyon SJ. 2009. *Ap. J.* 698:1–27

- Dahm SE, Carpenter JM. 2009. *A. J.* 137:4024–4045
- Dahm SE, Hillenbrand LA. 2007. *A. J.* 133:2072–2086
- Dai Y, Wilner DJ, Andrews SM, Ohashi N. 2010. *A. J.* 139:626–629
- D’Alessio P, Calvet N, Hartmann L. 2001. *Ap. J.* 553:321–334
- D’Alessio P, Calvet N, Hartmann L, Franco-Hernández R, Servín H. 2006. *Ap. J.* 638:314–335
- D’Alessio P, Calvet N, Hartmann L, Lizano S, Cantó J. 1999. *Ap. J.* 527:893–909
- D’Alessio P, Canto J, Calvet N, Lizano S. 1998. *Ap. J.* 500:411–+
- Damjanov I, Jayawardhana R, Scholz A, Ahmic M, Nguyen DC, et al. 2007. *Ap. J.* 670:1337–1346
- Dartois E, Dutrey A, Guilloteau S. 2003. *A&A* 399:773–787
- Davis SS. 2005. *Ap. J. Lett.* 627:L153–L155
- Desch SJ. 2007. *Ap. J.* 671:878–893
- Di Francesco J, Myers PC, Wilner DJ, Ohashi N, Mardones D. 2001. *Ap. J.* 562:770–789
- Dib S, Hennebelle P, Pineda JE, Csengeri T, Bontemps S, et al. 2010. *Ap. J.* 723:425–439
- D’Orazi V, Randich S, Flaccomio E, Palla F, Sacco GG, Pallavicini R. 2009. *A&A* 501:973–983
- Draine BT. 2003. *Ann. Rev. Astron. Astrophys.* 41:241–289
- Draine BT. 2006. *Ap. J.* 636:1114–1120
- Duchêne G. 2010. *Ap. J. Lett.* 709:L114–L118
- Dullemond CP, Dominik C. 2004. *A&A* 421:1075–1086
- Dullemond CP, Dominik C. 2005. *A&A* 434:971–986
- Dullemond CP, Dominik C. 2008. *A&A* 487:205–209
- Dullemond CP, Monnier JD. 2010. *Ann. Rev. Astron. Astrophys.* 48:205–239
- Dullemond CP, van Zadelhoff GJ, Natta A. 2002. *A&A* 389:464–474
- Dunham MM, Evans NJ, Terebey S, Dullemond CP, Young CH. 2010. *Ap. J.* 710:470–502
- Duquennoy A, Mayor M. 1991. *A&A* 248:485–524
- Dutrey A, Guilloteau S, Duvert G, Prato L, Simon M, et al. 1996. *A&A* 309:493–504
- Dutrey A, Guilloteau S, Guelin M. 1997. *A&A* 317:L55–L58
- Dutrey A, Guilloteau S, Piétu V, Chapillon E, Gueth F, et al. 2008. *A&A* 490:L15–L18
- Dutrey A, Guilloteau S, Simon M. 1994. *A&A* 286:149–159
- Dutrey A, Guilloteau S, Simon M. 2003. *A&A* 402:1003–1011
- Dutrey A, Henning T, Guilloteau S, Semenov D, Piétu V, et al. 2007. *A&A* 464:615–623
- Duvert G, Dutrey A, Guilloteau S, Menard F, Schuster K, et al. 1998. *A&A* 332:867–874

- Ehrenfreund P, Charnley SB. 2000. *Ann. Rev. Astron. Astrophys.* 38:427–483
- Eisner JA, Hillenbrand LA, Carpenter JM, Wolf S. 2005. *Ap. J.* 635:396–421
- Eisner JA, Plambeck RL, Carpenter JM, Corder SA, Qi C, Wilner D. 2008. *Ap. J.* 683:304–320
- Enoch ML, Corder S, Dunham MM, Duchêne G. 2009. *Ap. J.* 707:103–113
- Ercolano B, Clarke CJ. 2010. *MNRAS* 402:2735–2743
- Ercolano B, Clarke CJ, Robitaille TP. 2009. *MNRAS* 394:L141–L145
- Espaillat C, Calvet N, D’Alessio P, Hernández J, Qi C, et al. 2007. *Ap. J. Lett.* 670:L135–L138
- Espaillat C, D’Alessio P, Hernández J, Nagel E, Luhman KL, et al. 2010. *Ap. J.* 717:441–457
- Evans N, Calvet N, Cieza L, Forbrich J, Hillenbrand L, et al. 2009a. *ArXiv e-prints*
- Evans NJ, Dunham MM, Jørgensen JK, Enoch ML, Merín B, et al. 2009b. *Ap. J. Suppl.* 181:321–350
- Evans II NJ, Allen LE, Blake GA, Boogert ACA, Bourke T, et al. 2003. *PASP* 115:965–980
- Fang M, van Boekel R, Wang W, Carmona A, Sicilia-Aguilar A, Henning T. 2009. *A&A* 504:461–489
- Fedele D, van den Ancker ME, Henning T, Jayawardhana R, Oliveira JM. 2010. *A&A* 510:A72+
- Feigelson ED, Montmerle T. 1999. *Ann. Rev. Astron. Astrophys.* 37:363–408
- Fukagawa M, Hayashi M, Tamura M, Itoh Y, Hayashi SS, et al. 2004. *Ap. J. Lett.* 605:L53–L56
- Furlan E, Hartmann L, Calvet N, D’Alessio P, Franco-Hernández R, et al. 2006. *Ap. J. Suppl.* 165:568–605
- Furlan E, Watson DM, McClure MK, Manoj P, Espaillat C, et al. 2009. *Ap. J.* 703:1964–1983
- Garcia Lopez R, Natta A, Testi L, Habart E. 2006. *A&A* 459:837–842
- Gehrels T, ed. 1978. *Protostars and planets: Studies of star formation and of the origin of the solar system*
- Ghez AM, Neugebauer G, Matthews K. 1993. *A. J.* 106:2005–2023
- Girart JM, Rao R, Marrone DP. 2006. *Science* 313:812–814
- Glauser AM, Güdel M, Watson DM, Henning T, Schegerer AA, et al. 2009. *A&A* 508:247–257
- Goodman AA, Benson PJ, Fuller GA, Myers PC. 1993. *Ap. J.* 406:528–547
- Gorti U, Dullemond CP, Hollenbach D. 2009. *Ap. J.* 705:1237–1251
- Gorti U, Hollenbach D. 2009. *Ap. J.* 690:1539–1552
- Grady CA, Woodgate B, Bruhweiler FC, Boggess A, Plait P, et al. 1999. *Ap. J. Lett.* 523:L151–L154
- Greaves JS, Rice WKM. 2010. *MNRAS* 407:1981–1988
- Greene TP, Wilking BA, André P, Young ET, Lada CJ. 1994. *Ap. J.* 434:614–626

- Güdel M, Lahuis F, Briggs KR, Carr J, Glassgold AE, et al. 2010. *A&A* 519:A113+
- Guieu S, Pinte C, Monin J, Ménard F, Fukagawa M, et al. 2007. *A&A* 465:855–864
- Guilloteau S, Dutrey A. 1998. *A&A* 339:467–476
- Guilloteau S, Dutrey A, Pety J, Gueth F. 2008. *A&A* 478:L31–L34
- Guilloteau S, Dutrey A, Simon M. 1999. *A&A* 348:570–578
- Gutermuth RA, Myers PC, Megeath ST, Allen LE, Pipher JL, et al. 2008. *Ap. J.* 674:336–356
- Haisch Jr. KE, Lada EA, Lada CJ. 2001. *Ap. J. Lett.* 553:L153–L156
- Hartigan P, Edwards S, Ghandour L. 1995. *Ap. J.* 452:736–+
- Hartmann L. 2001. *A. J.* 121:1030–1039
- Hartmann L. 2009. *Accretion Processes in Star Formation: Second Edition.* Cambridge University Press
- Hartmann L, Calvet N, Gullbring E, D’Alessio P. 1998. *Ap. J.* 495:385–+
- Hartmann L, Kenyon SJ. 1996. *Ann. Rev. Astron. Astrophys.* 34:207–240
- Harvey P, Merín B, Huard TL, Rebull LM, Chapman N, et al. 2007. *Ap. J.* 663:1149–1173
- Heng K, Kenyon SJ. 2010. *MNRAS* :1234–+
- Henning T. 2010. *Ann. Rev. Astron. Astrophys.* 48:21–46
- Henning T, Semenov D, Guilloteau S, Dutrey A, Hersant F, et al. 2010. *Ap. J.* 714:1511–1520
- Herbig GH. 1977. *Ap. J.* 217:693–715
- Herczeg GJ, Linsky JL, Walter FM, Gahm GF, Johns-Krull CM. 2006. *Ap. J. Suppl.* 165:256–282
- Hernández J, Calvet N, Hartmann L, Muzerolle J, Gutermuth R, Stauffer J. 2009. *Ap. J.* 707:705–715
- Hernández J, Hartmann L, Calvet N, Jeffries RD, Gutermuth R, et al. 2008. *Ap. J.* 686:1195–1208
- Hernández J, Hartmann L, Megeath T, Gutermuth R, Muzerolle J, et al. 2007. *Ap. J.* 662:1067–1081
- Hillenbrand LA. 2005. *ArXiv Astrophysics e-prints*
- Hillenbrand LA. 2008. *Physica Scripta Volume T* 130:014024–+
- Hollenbach D, Johnstone D, Lizano S, Shu F. 1994. *Ap. J.* 428:654–669
- Hueso R, Guillot T. 2005. *A&A* 442:703–725
- Hughes AM, Andrews SM, Espaillat C, Wilner DJ, Calvet N, et al. 2009a. *Ap. J.* 698:131–142
- Hughes AM, Wilner DJ, Andrews SM, Qi C, Hogerheijde MR. 2010. *ArXiv e-prints*
- Hughes AM, Wilner DJ, Cho J, Marrone DP, Lazarian A, et al. 2009b. *Ap. J.* 704:1204–1217

- Hughes AM, Wilner DJ, Qi C, Hogerheijde MR. 2008. *Ap. J.* 678:1119–1126
- Ireland MJ, Kraus AL. 2008. *Ap. J. Lett.* 678:L59–L62
- Isella A, Carpenter JM, Sargent AI. 2009. *Ap. J.* 701:260–282
- Isella A, Carpenter JM, Sargent AI. 2010. *Ap. J.* 714:1746–1761
- Isella A, Testi L, Natta A, Neri R, Wilner D, Qi C. 2007. *A&A* 469:213–222
- Jensen ELN, Mathieu RD, Fuller GA. 1994. *Ap. J. Lett.* 429:L29–L32
- Jensen ELN, Mathieu RD, Fuller GA. 1996. *Ap. J.* 458:312–+
- Jewitt D, Luu J, Trujillo C. 1998. *A. J.* 115:2125–2135
- Johansen A, Youdin A, Mac Low M. 2009. *Ap. J. Lett.* 704:L75–L79
- Johnson JA. 2009. *PASP* 121:309–315
- Jørgensen JK, Bourke TL, Myers PC, Di Francesco J, van Dishoeck EF, et al. 2007. *Ap. J.* 659:479–498
- Jørgensen JK, Bourke TL, Myers PC, Schöier FL, van Dishoeck EF, Wilner DJ. 2005a. *Ap. J.* 632:973–981
- Jørgensen JK, Lahuis F, Schöier FL, van Dishoeck EF, Blake GA, et al. 2005b. *Ap. J. Lett.* 631:L77–L80
- Jørgensen JK, van Dishoeck EF. 2010. *Ap. J. Lett.* 710:L72–L76
- Jørgensen JK, van Dishoeck EF, Visser R, Bourke TL, Wilner DJ, et al. 2009. *A&A* 507:861–879
- Kamp I, Freudling W, Chengalur JN. 2007. *Ap. J.* 660:469–478
- Kamp I, Freudling W, Robberto M, Chengalur J, Keto E. 2008. *Physica Scripta Volume T* 130:014013–+
- Keene J, Masson CR. 1990. *Ap. J.* 355:635–644
- Kenyon SJ, Hartmann L. 1987. *Ap. J.* 323:714–733
- Kenyon SJ, Hartmann LW, Strom KM, Strom SE. 1990. *A. J.* 99:869–887
- Kessler-Silacci J, Augereau J, Dullemond CP, Geers V, Lahuis F, et al. 2006. *Ap. J.* 639:275–291
- Kessler-Silacci JE, Dullemond CP, Augereau J, Merín B, Geers VC, et al. 2007. *Ap. J.* 659:680–684
- Kim KH, Watson DM, Manoj P, Furlan E, Najita J, et al. 2009. *Ap. J.* 700:1017–1025
- Kitamura Y, Momose M, Yokogawa S, Kawabe R, Tamura M, Ida S. 2002. *Ap. J.* 581:357–380
- Koerner DW, Sargent AI, Beckwith SVW. 1993. *Icarus* 106:2–+
- Kohler R, Leinert C. 1998. *A&A* 331:977–988
- Kusaka T, Nakano T, Hayashi C. 1970. *Progress of Theoretical Physics* 44:1580–1595
- Kwon W, Looney LW, Mundy LG, Chiang H, Kemball AJ. 2009. *Ap. J.* 696:841–852
- Lada CJ. 1987. In *Star Forming Regions*, ed. M. Peimbert & J. Jugaku, vol. 115 of *IAU Symposium*

- Lada CJ, Lada EA. 2003. *Ann. Rev. Astron. Astrophys.* 41:57–115
- Lada CJ, Muench AA, Luhman KL, Allen L, Hartmann L, et al. 2006. *A. J.* 131:1574–1607
- Lada CJ, Wilking BA. 1984. *Ap. J.* 287:610–621
- Lahuis F, van Dishoeck EF, Blake GA, Evans II NJ, Kessler-Silacci JE, Pontoppidan KM. 2007. *Ap. J.* 665:492–511
- Lahuis F, van Dishoeck EF, Boogert ACA, Pontoppidan KM, Blake GA, et al. 2006. *Ap. J. Lett.* 636:L145–L148
- Laughlin G, Bodenheimer P. 1994. *Ap. J.* 436:335–354
- Lay OP, Carlstrom JE, Hills RE. 1997. *Ap. J.* 489:917–+
- Leinert C, Zinnecker H, Weitzel N, Christou J, Ridgway ST, et al. 1993. *A&A* 278:129–149
- Levy EH, Lunine JJ, eds. 1993. *Protostars and planets III*
- Li A, Draine BT. 2001. *Ap. J.* 554:778–802
- Lin S, Ohashi N, Lim J, Ho PTP, Fukagawa M, Tamura M. 2006. *Ap. J.* 645:1297–1304
- Lommen D, Jørgensen JK, van Dishoeck EF, Crapsi A. 2008. *A&A* 481:141–147
- Lommen D, Maddison ST, Wright CM, van Dishoeck EF, Wilner DJ, Bourke TL. 2009. *A&A* 495:869–879
- Lommen D, Wright CM, Maddison ST, Jørgensen JK, Bourke TL, et al. 2007. *A&A* 462:211–220
- Looney LW, Mundy LG, Welch WJ. 2000. *Ap. J.* 529:477–498
- Looney LW, Mundy LG, Welch WJ. 2003. *Ap. J.* 592:255–265
- Luhman KL, Lada CJ, Hartmann L, Muench AA, Megeath ST, et al. 2005. *Ap. J. Lett.* 631:L69–L72
- Lynden-Bell D, Pringle JE. 1974. *MNRAS* 168:603–637
- Mamajek EE. 2009. In *American Institute of Physics Conference Series*, ed. T. Usuda, M. Tamura, & M. Ishii, vol. 1158 of *American Institute of Physics Conference Series*
- Mann RK, Williams JP. 2009a. *Ap. J. Lett.* 699:L55–L58
- Mann RK, Williams JP. 2009b. *Ap. J. Lett.* 694:L36–L40
- Mann RK, Williams JP. 2010. *Ap. J.* 725:430–442
- Mannings V, Boss AP, Russell SS. 2000. *Protostars and Planets IV*
- Mannings V, Emerson JP. 1994. *MNRAS* 267:361–378
- Mannings V, Koerner DW, Sargent AI. 1997. *Nature* 388:555–557
- Mannings V, Sargent AI. 2000. *Ap. J.* 529:391–401
- Martin-Zaïdi C, Augereau J, Ménard F, Olofsson J, Carmona A, et al. 2010. *A&A* 516:A110+
- Martin-Zaïdi C, Lagage P, Pantin E, Habart E. 2007. *Ap. J. Lett.* 666:L117–L120
- Mathews GS, Dent WRF, Williams JP, Howard CD, Meeus G, et al. 2010. *A&A* 518:L127+

- Mathis JS, Rumpl W, Nordsieck KH. 1977. *Ap. J.* 217:425–433
- McCaughrean MJ, Chen H, Bally J, Erickson E, Thompson R, et al. 1998. *Ap. J. Lett.* 492:L157+
- McCaughrean MJ, O’dell CR. 1996. *A. J.* 111:1977–+
- McClure MK, Furlan E, Manoj P, Luhman KL, Watson DM, et al. 2010. *Ap. J. Suppl.* 188:75–122
- McKee CF, Williams JP. 1997. *Ap. J.* 476:144–+
- Meijerink R, Pontoppidan KM, Blake GA, Poelman DR, Dullemond CP. 2009. *Ap. J.* 704:1471–1481
- Merín B, Brown JM, Oliveira I, Herczeg GJ, van Dishoeck EF, et al. 2010. *Ap. J.* 718:1200–1223
- Meyer MR, Hillenbrand LA, Backman D, Beckwith S, Bouwman J, et al. 2006. *PASP* 118:1690–1710
- Monin J, Guieu S, Pinte C, Rebull L, Goldsmith P, et al. 2010. *A&A* 515:A91+
- Mouillet D, Larwood JD, Papaloizou JCB, Lagrange AM. 1997. *MNRAS* 292:896–+
- Mundy LG, Looney LW, Erickson W, Grossman A, Welch WJ, et al. 1996. *Ap. J. Lett.* 464:L169+
- Muzerolle J, Allen LE, Megeath ST, Hernández J, Gutermuth RA. 2010. *Ap. J.* 708:1107–1118
- Muzerolle J, Calvet N, Hartmann L. 1998. *Ap. J.* 492:743–+
- Najita JR, Carr JS, Glassgold AE, Valenti JA. 2007. *Protostars and Planets V* :507–522
- Najita JR, Strom SE, Muzerolle J. 2007. *MNRAS* 378:369–378
- Narayanan D, Kulesa CA, Boss A, Walker CK. 2006. *Ap. J.* 647:1426–1436
- Natta A, Grinin V, Mannings V. 2000. *Protostars and Planets IV* :559–+
- Natta A, Testi L, Neri R, Shepherd DS, Wilner DJ. 2004. *A&A* 416:179–186
- Öberg KI, Qi C, Fogel JKJ, Bergin EA, Andrews SM, et al. 2010. *Ap. J.* 720:480–493
- O’dell CR, Wen Z. 1994. *Ap. J.* 436:194–202
- Olczak C, Pfalzner S, Spurzem R. 2006. *Ap. J.* 642:1140–1151
- Oliveira I, Pontoppidan KM, Merín B, van Dishoeck EF, Lahuis F, et al. 2010. *Ap. J.* 714:778–798
- Olofsson J, Augereau J, van Dishoeck EF, Merín B, Lahuis F, et al. 2009. *A&A* 507:327–345
- Ossenkopf V, Henning T. 1994. *A&A* 291:943–959
- Osterloh M, Beckwith SVW. 1995. *Ap. J.* 439:288–302
- Owen JE, Ercolano B, Clarke CJ, Alexander RD. 2010. *MNRAS* 401:1415–1428
- Padgett DL, Brandner W, Stapelfeldt KR, Strom SE, Terebey S, Koerner D. 1999. *A. J.* 117:1490–1504
- Padgett DL, Cieza L, Stapelfeldt KR, Evans II NJ, Koerner D, et al. 2006. *Ap. J.* 645:1283–1296

- Pagani L, Steinacker J, Bacmann A, Stutz A, Henning T. 2010. *Science* 329:1622–
- Panić O, Hogerheijde MR. 2009. *A&A* 508:707–716
- Panić O, Hogerheijde MR, Wilner D, Qi C. 2008. *A&A* 491:219–227
- Papaloizou J, Pringle JE. 1977. *MNRAS* 181:441–454
- Pascucci I, Apai D, Luhman K, Henning T, Bouwman J, et al. 2009. *Ap. J.* 696:143–159
- Pascucci I, Sterzik M. 2009. *Ap. J.* 702:724–732
- Piétu V, Dutrey A, Guilloteau S. 2007. *A&A* 467:163–178
- Piétu V, Dutrey A, Guilloteau S, Chapillon E, Pety J. 2006. *A&A* 460:L43–L47
- Piétu V, Guilloteau S, Dutrey A. 2005. *A&A* 443:945–954
- Pinte C, Ménard F, Berger JP, Benisty M, Malbet F. 2008. *Ap. J. Lett.* 673:L63–L66
- Pollack JB, Hollenbach D, Beckwith S, Simonelli DP, Roush T, Fong W. 1994. *Ap. J.* 421:615–639
- Pontoppidan KM, Blake GA, van Dishoeck EF, Smette A, Ireland MJ, Brown J. 2008. *Ap. J.* 684:1323–1329
- Pontoppidan KM, Salyk C, Blake GA, Meijerink R, Carr JS, Najita J. 2010. *Ap. J.* 720:887–903
- Pott J, Perrin MD, Furlan E, Ghez AM, Herbst TM, Metchev S. 2010. *Ap. J.* 710:265–278
- Preibisch T, Mamajek E. 2008. *The Nearest OB Association: Scorpius-Centaurus (Sco OB2)*. 235–+
- Qi C, Ho PTP, Wilner DJ, Takakuwa S, Hirano N, et al. 2004. *Ap. J. Lett.* 616:L11–L14
- Qi C, Kessler JE, Koerner DW, Sargent AI, Blake GA. 2003. *Ap. J.* 597:986–997
- Qi C, Wilner DJ, Aikawa Y, Blake GA, Hogerheijde MR. 2008. *Ap. J.* 681:1396–1407
- Qi C, Wilner DJ, Calvet N, Bourke TL, Blake GA, et al. 2006. *Ap. J. Lett.* 636:L157–L160
- Raghavan D, McAlister HA, Henry TJ, Latham DW, Marcy GW, et al. 2010. *Ap. J. Suppl.* 190:1–42
- Ratzka T, Köhler R, Leinert C. 2005. *A&A* 437:611–626
- Reipurth B, Jewitt D, Keil K. 2007. *Protostars and Planets V*
- Riaz B, Gizis JE. 2008. *Ap. J.* 681:1584–1592
- Riaz B, Lodieu N, Gizis JE. 2009. *Ap. J.* 705:1173–1182
- Ricci L, Mann RK, Testi L, Williams JP, Isella A, et al. 2011. *A&A* 525:A81+
- Ricci L, Testi L, Natta A, Brooks KJ. 2010a. *A&A* 521:A66+
- Ricci L, Testi L, Natta A, Neri R, Cabrit S, Herczeg GJ. 2010b. *A&A* 512:A15+
- Robitaille TP, Whitney BA, Indebetouw R, Wood K, Denzmore P. 2006. *Ap. J. Suppl.* 167:256–285
- Rodmann J, Henning T, Chandler CJ, Mundy LG, Wilner DJ. 2006. *A&A* 446:211–221

- Rodríguez LF, D'Alessio P, Wilner DJ, Ho PTP, Torrelles JM, et al. 1998. *Nature* 395:355–357
- Salyk C, Pontoppidan KM, Blake GA, Lahuis F, van Dishoeck EF, Evans II NJ. 2008. *Ap. J. Lett.* 676:L49–L52
- Sandford SA, Allamandola LJ. 1993. *Ap. J.* 417:815–825
- Sargent AI, Beckwith S. 1987. *Ap. J.* 323:294–305
- Scally A, Clarke C. 2001. *MNRAS* 325:449–456
- Schaefer GH, Dutrey A, Guilloteau S, Simon M, White RJ. 2009. *Ap. J.* 701:698–709
- Scholz A, Jayawardhana R, Wood K. 2006. *Ap. J.* 645:1498–1508
- Scholz A, Jayawardhana R, Wood K, Meeus G, Stelzer B, et al. 2007. *Ap. J.* 660:1517–1531
- Shirley YL, Evans II NJ, Rawlings JMC, Gregersen EM. 2000. *Ap. J. Suppl.* 131:249–271
- Sicilia-Aguilar A, Hartmann L, Calvet N, Megeath ST, Muzerolle J, et al. 2006. *Ap. J.* 638:897–919
- Sicilia-Aguilar A, Henning T, Hartmann LW. 2010. *Ap. J.* 710:597–612
- Sicilia-Aguilar A, Henning T, Juhász A, Bouwman J, Garmire G, Garmire A. 2008. *Ap. J.* 687:1145–1167
- Simon M, Dutrey A, Guilloteau S. 2000. *Ap. J.* 545:1034–1043
- Skrutskie MF, Dutkevitch D, Strom SE, Edwards S, Strom KM, Shure MA. 1990. *A. J.* 99:1187–1195
- Smith N, Bally J, Licht D, Walawender J. 2005. *A. J.* 129:382–392
- Smith N, Bally J, Morse JA. 2003. *Ap. J. Lett.* 587:L105–L108
- Stapelfeldt KR, Krist JE, Menard F, Bouvier J, Padgett DL, Burrows CJ. 1998. *Ap. J. Lett.* 502:L65+
- Störzer H, Hollenbach D. 1999. *Ap. J.* 515:669–684
- Strom KM, Strom SE, Edwards S, Cabrit S, Skrutskie MF. 1989. *A. J.* 97:1451–1470
- Sturm B, Bouwman J, Henning T, Evans NJ, Acke B, et al. 2010. *A&A* 518:L129+
- Sung H, Stauffer JR, Bessell MS. 2009. *A. J.* 138:1116–1136
- Szűcs L, Apai D, Pascucci I, Dullemond CP. 2010. *Ap. J.* 720:1668–1673
- Tamura M, Hough JH, Greaves JS, Morino J, Chrysostomou A, et al. 1999. *Ap. J.* 525:832–836
- Terebey S, Shu FH, Cassen P. 1984. *Ap. J.* 286:529–551
- Thalmann C, Grady CA, Goto M, Wisniewski JP, Janson M, et al. 2010. *Ap. J. Lett.* 718:L87–L91
- Thi W, Mathews G, Ménard F, Woitke P, Meeus G, et al. 2010. *A&A* 518:L125+
- Thi W, van Zadelhoff G, van Dishoeck EF. 2004. *A&A* 425:955–972
- Throop HB, Bally J. 2005. *Ap. J. Lett.* 623:L149–L152
- Throop HB, Bally J, Esposito LW, McCaughrean MJ. 2001. *Science* 292:1686–1698

- Tielens AGGM. 2008. *Ann. Rev. Astron. Astrophys.* 46:289–337
- Toomre A. 1964. *Ap. J.* 139:1217–1238
- Turner NJ, Drake JF. 2009. *Ap. J.* 703:2152–2159
- Valenti JA, Fischer DA. 2005. *Ap. J. Suppl.* 159:141–166
- van Zadelhoff G, van Dishoeck EF, Thi W, Blake GA. 2001. *A&A* 377:566–580
- Vicente SM, Alves J. 2005. *A&A* 441:195–205
- Vorobyov EI, Basu S. 2010. *Ap. J.* 719:1896–1911
- Wahhaj Z, Cieza L, Koerner DW, Stapelfeldt KR, Padgett DL, et al. 2010. *Ap. J.* 724:835–854
- Watson DM, Bohac CJ, Hull C, Forrest WJ, Furlan E, et al. 2007. *Nature* 448:1026–1028
- Weidenschilling SJ. 1977. *MNRAS* 180:57–70
- Weintraub DA, Sandell G, Duncan WD. 1989. *Ap. J. Lett.* 340:L69–L72
- White RJ, Basri G. 2003. *Ap. J.* 582:1109–1122
- Wilner DJ. 2004. *New Astron. Rev.* 48:1363–1375
- Wilner DJ, D’Alessio P, Calvet N, Claussen MJ, Hartmann L. 2005. *Ap. J. Lett.* 626:L109–L112
- Wilner DJ, Ho PTP, Kastner JH, Rodríguez LF. 2000. *Ap. J. Lett.* 534:L101–L104
- Winston E, Megeath ST, Wolk SJ, Muzerolle J, Gutermuth R, et al. 2007. *Ap. J.* 669:493–518
- Woitke P, Kamp I, Thi W. 2009. *A&A* 501:383–406
- Wolf S, D’Angelo G. 2005. *Ap. J.* 619:1114–1122
- Wolk SJ, Walter FM. 1996. *A. J.* 111:2066–+
- Wyatt MC. 2008. *Ann. Rev. Astron. Astrophys.* 46:339–383
- Yasui C, Kobayashi N, Tokunaga AT, Saito M, Tokoku C. 2009. *Ap. J.* 705:54–63
- Yasui C, Kobayashi N, Tokunaga AT, Saito M, Tokoku C. 2010. *Ap. J. Lett.* 723:L113–L116
- Yorke HW, Bodenheimer P, Laughlin G. 1993. *Ap. J.* 411:274–284
- Youdin AN, Shu FH. 2002. *Ap. J.* 580:494–505
- Young CH, Shirley YL, Evans II NJ, Rawlings JMC. 2003. *Ap. J. Suppl.* 145:111–145
- Zhu Z, Hartmann L, Gammie C, McKinney JC. 2009. *Ap. J.* 701:620–634
- Zinnecker H, Yorke HW. 2007. *Ann. Rev. Astron. Astrophys.* 45:481–563

Table 1: Classification of Young Stellar Objects

Class	SED slope	Physical properties	Observational characteristics
0	–	$M_{\text{env}} > M_{\text{star}} > M_{\text{disk}}$	no optical or near-infrared emission
I	$\alpha_{\text{IR}} > 0.3$	$M_{\text{star}} > M_{\text{env}} \sim M_{\text{disk}}$	generally optically obscured
FS	$-0.3 < \alpha_{\text{IR}} < 0.3$		intermediate between Class I and II
II	$-1.6 < \alpha_{\text{IR}} < -0.3$	$M_{\text{disk}}/M_{\text{star}} \sim 1\%, M_{\text{env}} \sim 0$	accreting disk; strong H α and UV
III	$\alpha_{\text{IR}} < -1.6$	$M_{\text{disk}}/M_{\text{star}} \ll 1\%, M_{\text{env}} \sim 0$	passive disk; no or very weak accretion

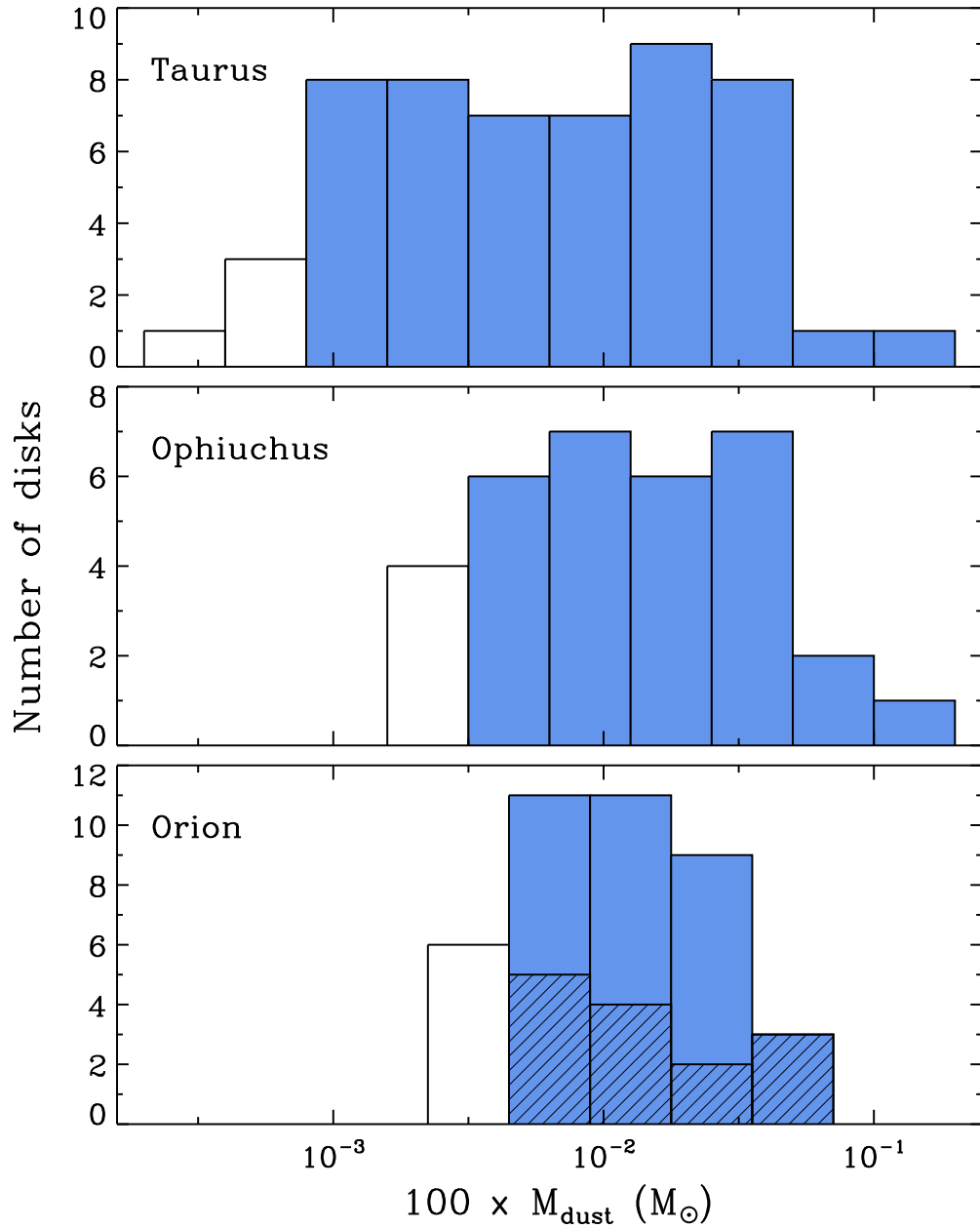


Figure 1: The distribution of protoplanetary (Class II) disk masses in Taurus, Ophiuchus, and Orion. The dust masses are derived from millimeter fluxes and extrapolated to a total mass assuming a maximum grain size of 1 mm, characteristic temperature of 20 K, and an interstellar gas-to-dust ratio of 100 (Andrews & Williams 2005, 2007a, Mann & Williams 2010). The filled bars show the range where the millimeter measurements are complete for each region. The hashed bars in the Orion histogram show the disks with projected distances 0.3 pc beyond the O6 star, θ^1 Ori C, in the Trapezium Cluster.

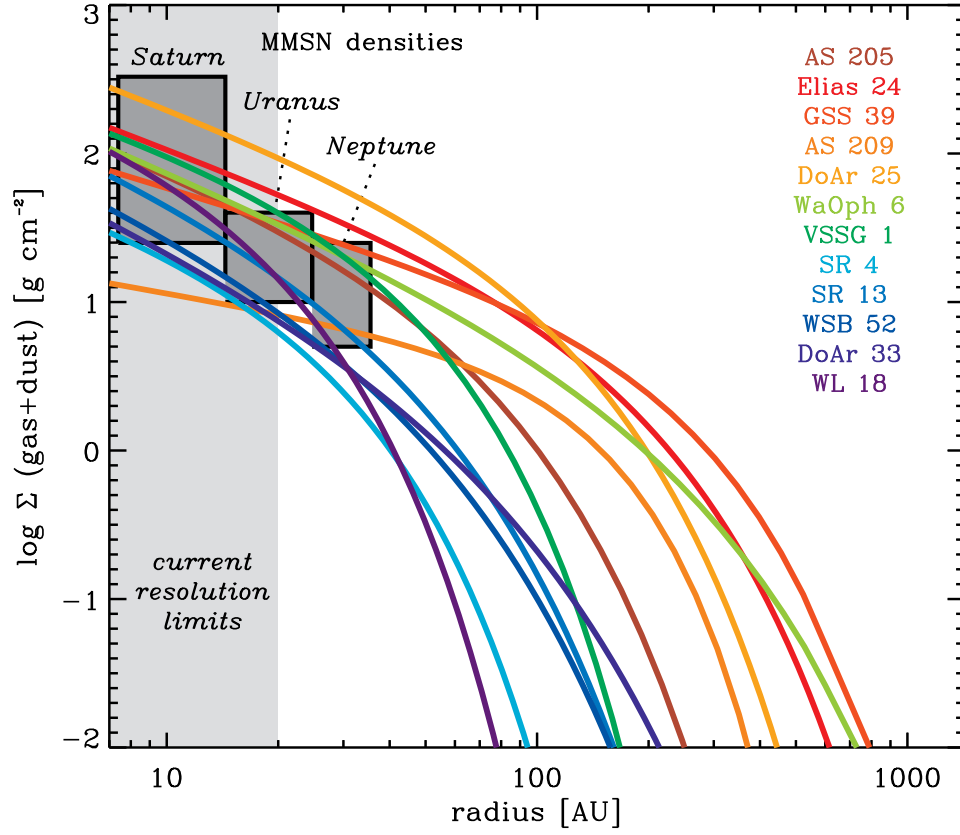


Figure 2: Radial surface density (gas+dust) profiles for Class II YSO disks in Ophiuchus based on fitting an exponentially tapered power law profile to $880\,\mu\text{m}$ visibilities and infrared SEDs (Andrews et al. 2009) and Andrews et al. (2010b). The dark gray rectangular regions mark the MMSN surface densities for Saturn, Uranus, and Neptune.

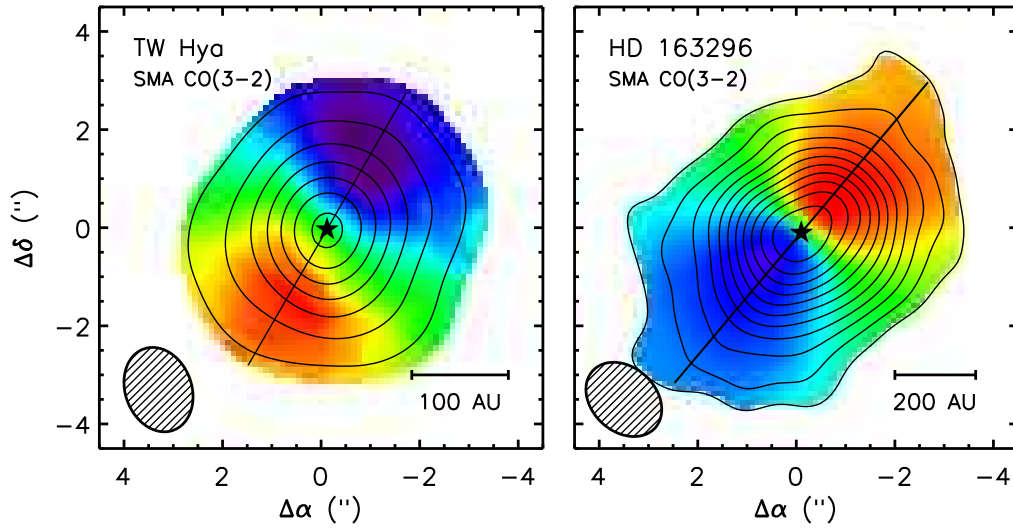


Figure 3: CO(3-2) emission from the disks around TW Hydra (left) and HD 163296 (right) observed with the SMA at a spectral resolution of 44 ms^{-1} (Hughes et al. 2010). The contours show the zeroth moment (velocity-integrated intensity), whereas the colors show the first moment (intensity-weighted velocity). The synthesized beams are shown in the lower left corner of each panel with a size of $1''.7 \times 1''.3$ at position angles of 19° and 46° degrees for TW Hydra and HD 163296, respectively. The contours start at 3σ and increase by intervals of 2σ , where the rms noise $\sigma = 0.6 \text{ Jy beam}^{-1}$.

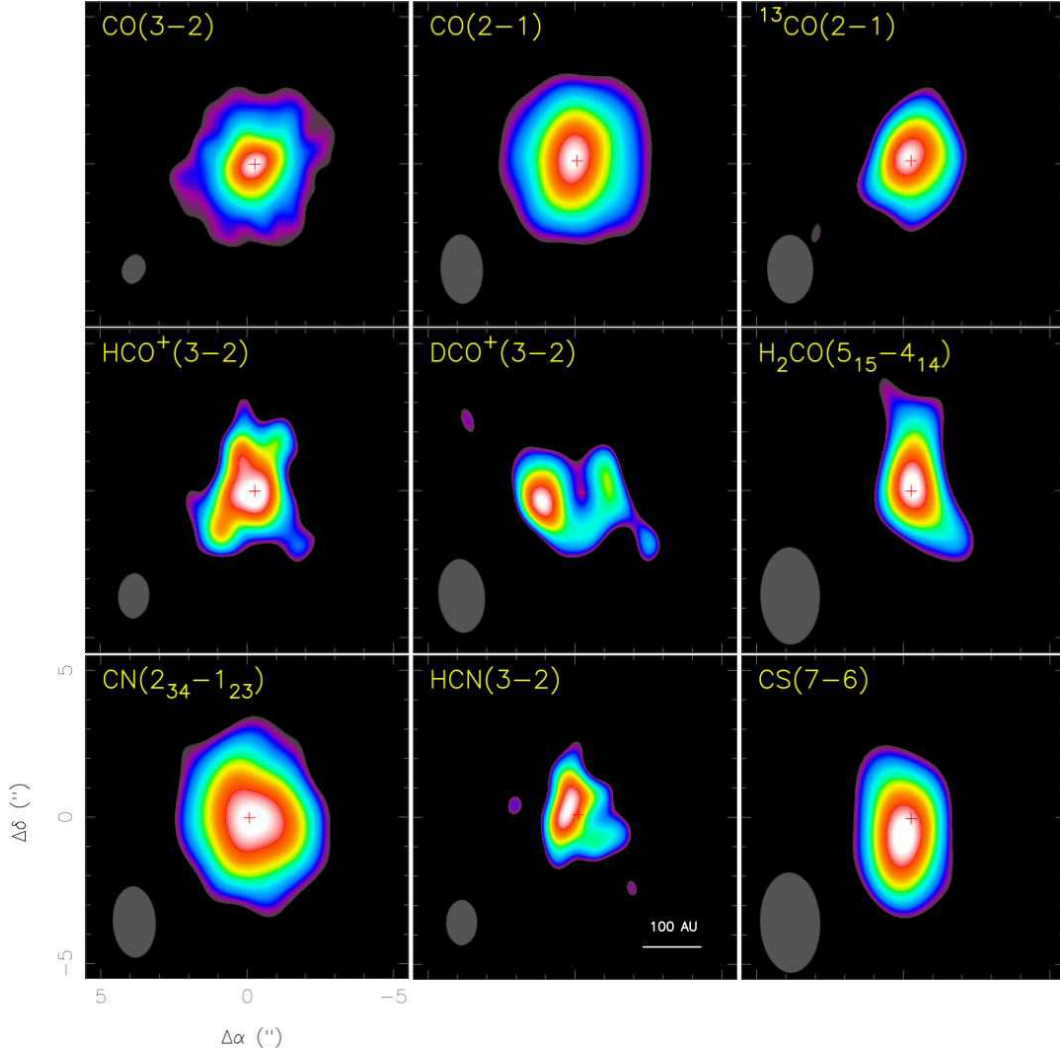


Figure 4: Sub-millimeter spectroscopy of molecular rotational lines in the chemically rich nearby TW Hydra disk. These observations, made with the *SMA* are at a range of resolutions, shown in the lower left corner of each panel. The nearly face-on disk generally shows centrally peaked emission except for the DCO^+ line which peaks in a ring where the temperature is colder than the inner disk and CO freezes out of the gas phase onto grain surfaces. (Figure courtesy of Charlie Qi.)

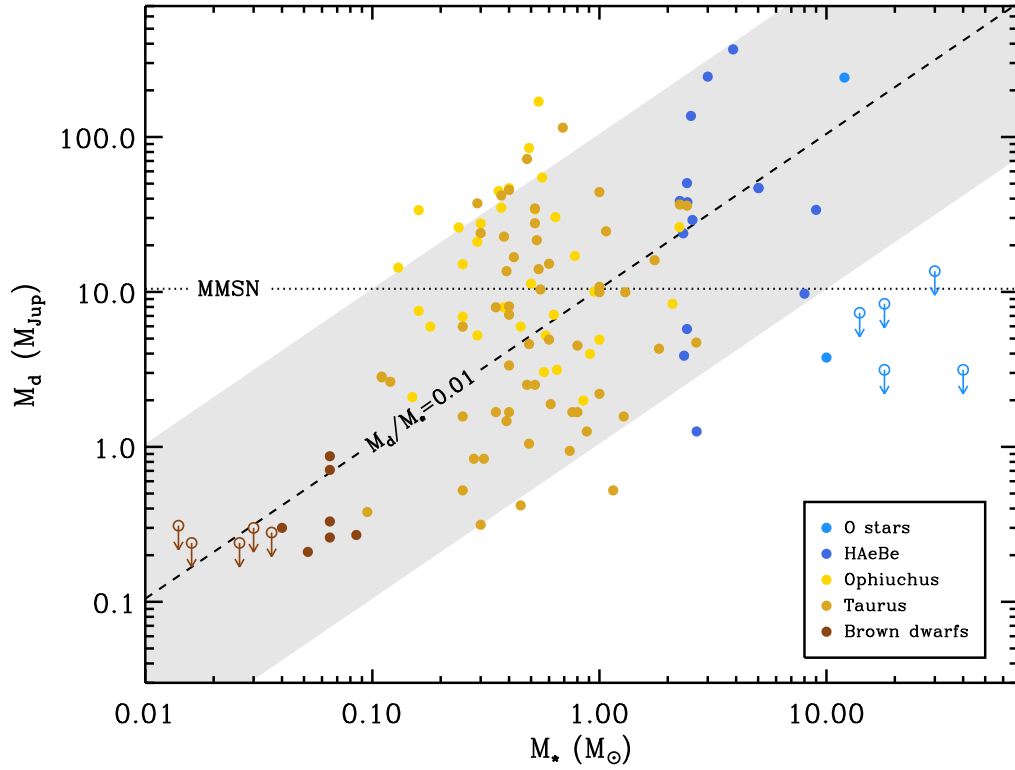


Figure 5: The variation of protoplanetary disk mass with the mass of the central star. Upper limits are only shown at the extremes of the stellar mass range where no disks have been detected. The dashed diagonal lines delineates where the mass ratio is 1%, and is close to the median of the detections. Almost all the disks around stars with masses $M_* = 0.04 - 10 M_\odot$ lie within the grey shaded area, ± 1 dex, about the median. The exception are O stars where no disks are detected at (sub-)millimeter wavelengths, indicating either very short disk lifetimes or a different star formation scenario.

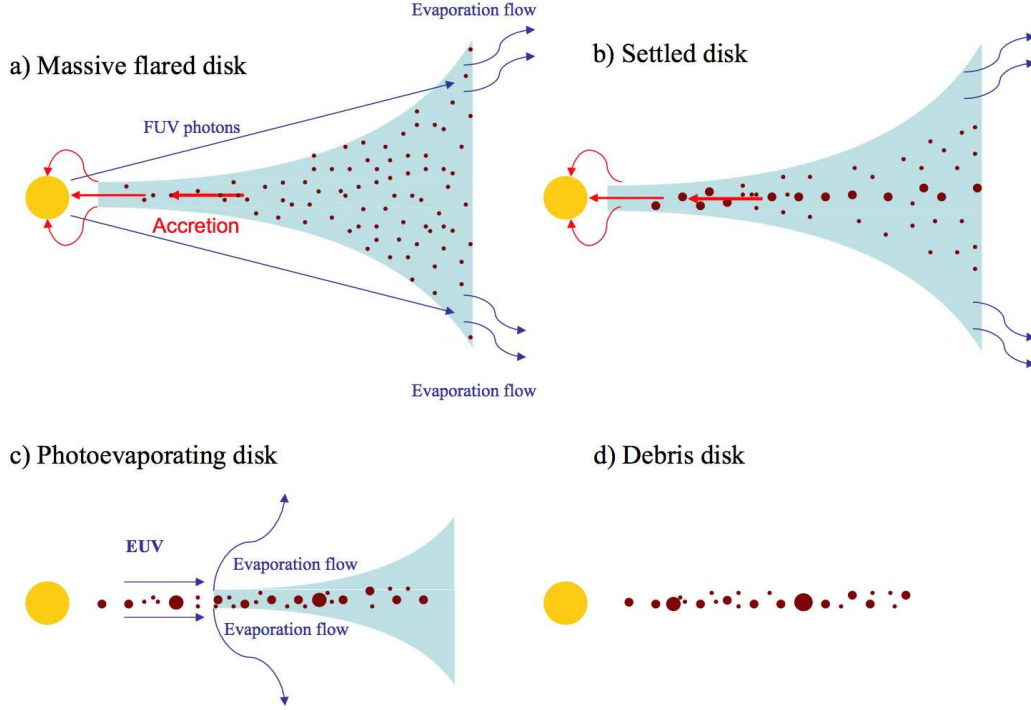


Figure 6: The evolution of a typical disk. The gas distribution is shown in blue and the dust in brown. (a) Early in its evolution, the disk loses mass through accretion onto the star and FUV photoevaporation of the outer disk. (b) At the same time, grains grow into larger bodies that settle to the mid-plane of the disk. (c) As the disk mass and accretion rate decrease, EUV-induced photoevaporation becomes important, the outer disk is no longer able to resupply the inner disk with material, and the inner disk drains on a viscous timescale ($\sim 10^5$ yr). An inner hole is formed, accretion onto the star ceases, and the disk quickly dissipates from the inside out. (d) Once the remaining gas photoevaporates, the small grains are removed by radiation pressure and Poynting-Robertson drag. Only large grains, planetesimals, and/or planets are left. This debris disk is very low mass and is not always detectable.

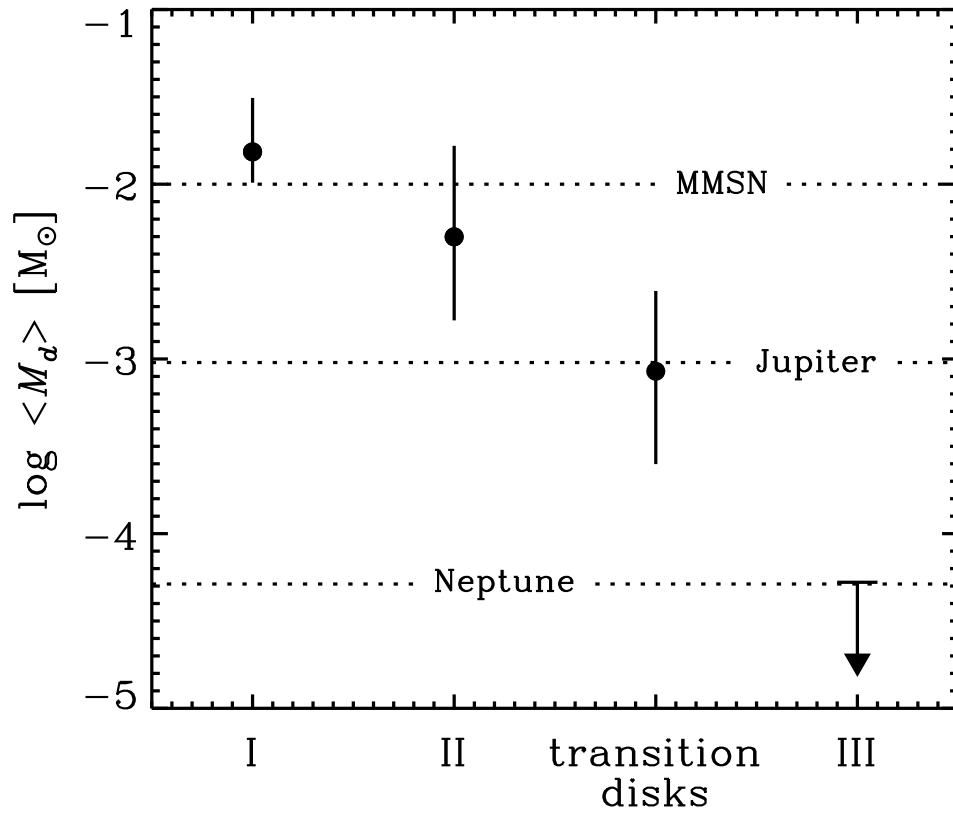


Figure 7: Evolution of the disk masses across the empirical sequence defined by the slope of the infrared SED. The circles show the median disk mass, as measured at sub-millimeter wavelengths for a sample of 300 YSOs in Taurus and Ophiuchus. Error bars show the distribution quartiles. Transition disks are defined here as those YSOs that lack infrared excesses for wavelengths less than $25 \mu\text{m}$, but have detectable sub-millimeter emission. With this definition, no Class III YSO was detected and the stringent limit to their median mass comes from stacking the non-detections together (Andrews & Williams 2007a).

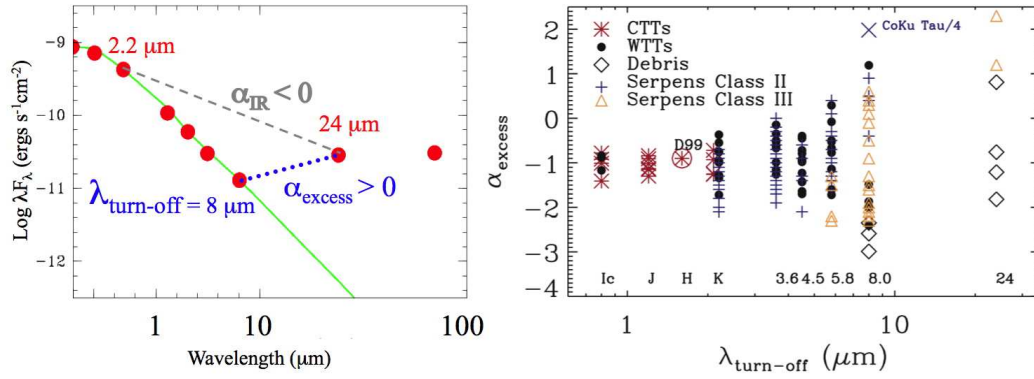


Figure 8: (a) A schematic of the α_{excess} and $\lambda_{\text{turn-off}}$ classification for a transition disk. Although the α_{IR} value is typical of a CTTS with a full disk, the long $\lambda_{\text{turn-off}}$ wavelength and positive α_{excess} indicate the presence of an inner hole. (b) Distribution of α_{excess} with respect to $\lambda_{\text{turn-off}}$ for a range of different disk evolutionary types (Harvey et al. 2007). The diagram demonstrates the increasing range of possible α_{excess} values at longer $\lambda_{\text{turn-off}}$ wavelengths due to the diversity of transition disk SED morphologies.

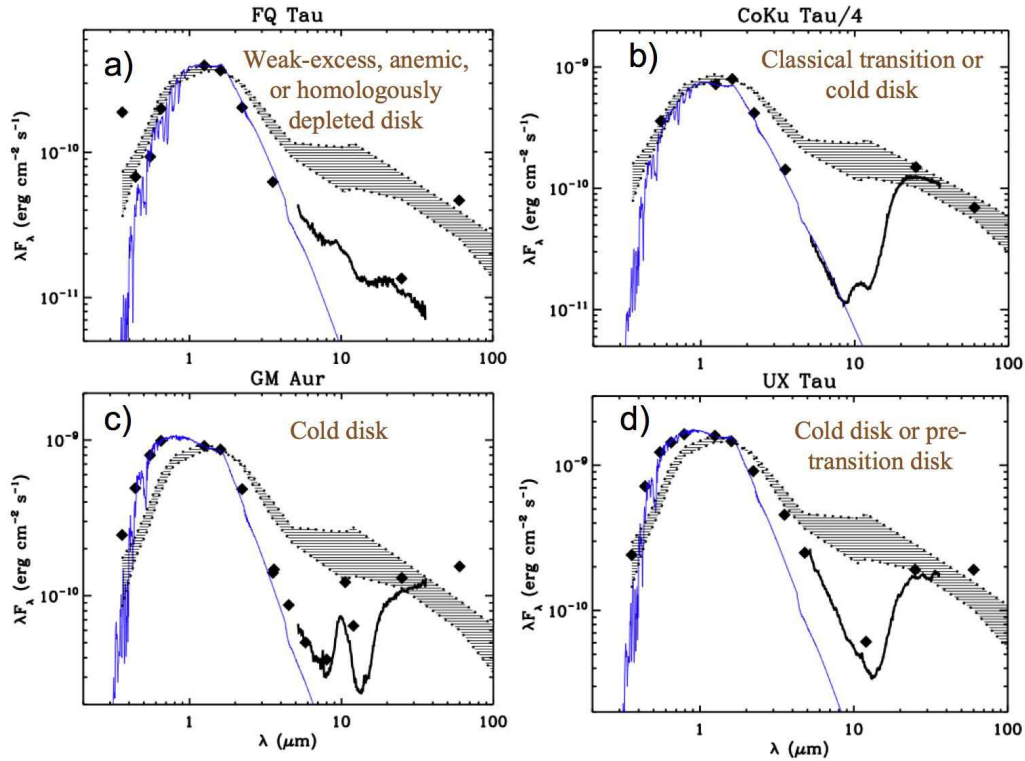


Figure 9: The diversity of transition disks SEDs. The points represent photometry from optical to mid-infrared wavelengths, whereas the dark solid lines are *Spitzer* infrared spectra. The stellar photosphere is shown as a blue curve, and the dark hashed region shows the range of SEDs for typical accreting T Tauri stars. (a) A weak-excess, anemic, or homologously depleted disk has a significant flux decrement at all mid-infrared wavelengths relative to the T Tauri SED. (b) A cold disk or “classical” transition disk displays excess emission above the photosphere only at mid-infrared wavelengths and beyond. (c) A cold disk with little near-infrared emission and a strong $10\,\mu\text{m}$ silicate feature. (d) A cold disk with near-infrared excess emission. This can also be considered a pre-transition disk because its SED can be modeled with an optically thin gap separating optically thick inner and outer disk components. Figure adapted from Najita, Strom & Muzerolle (2007).

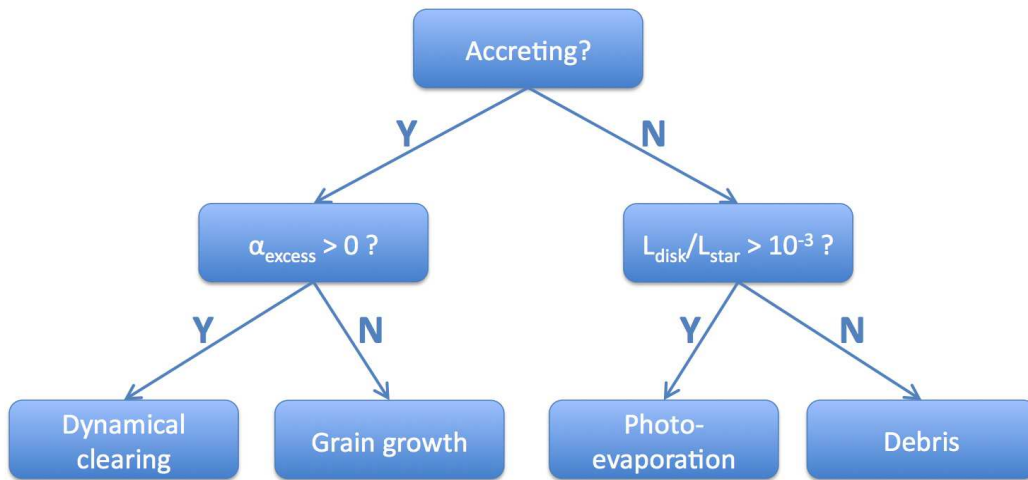


Figure 10: Decision tree to determine the dominant physical process for transition disks, defined as having a significant flux decrement relative to the median SED of CTTS at any or all infrared wavelengths. This appears to be an exhaustive set of possibilities for transition disks in Ophiuchus (Cieza et al. 2010) but there may be rare additional possibilities in other regions.

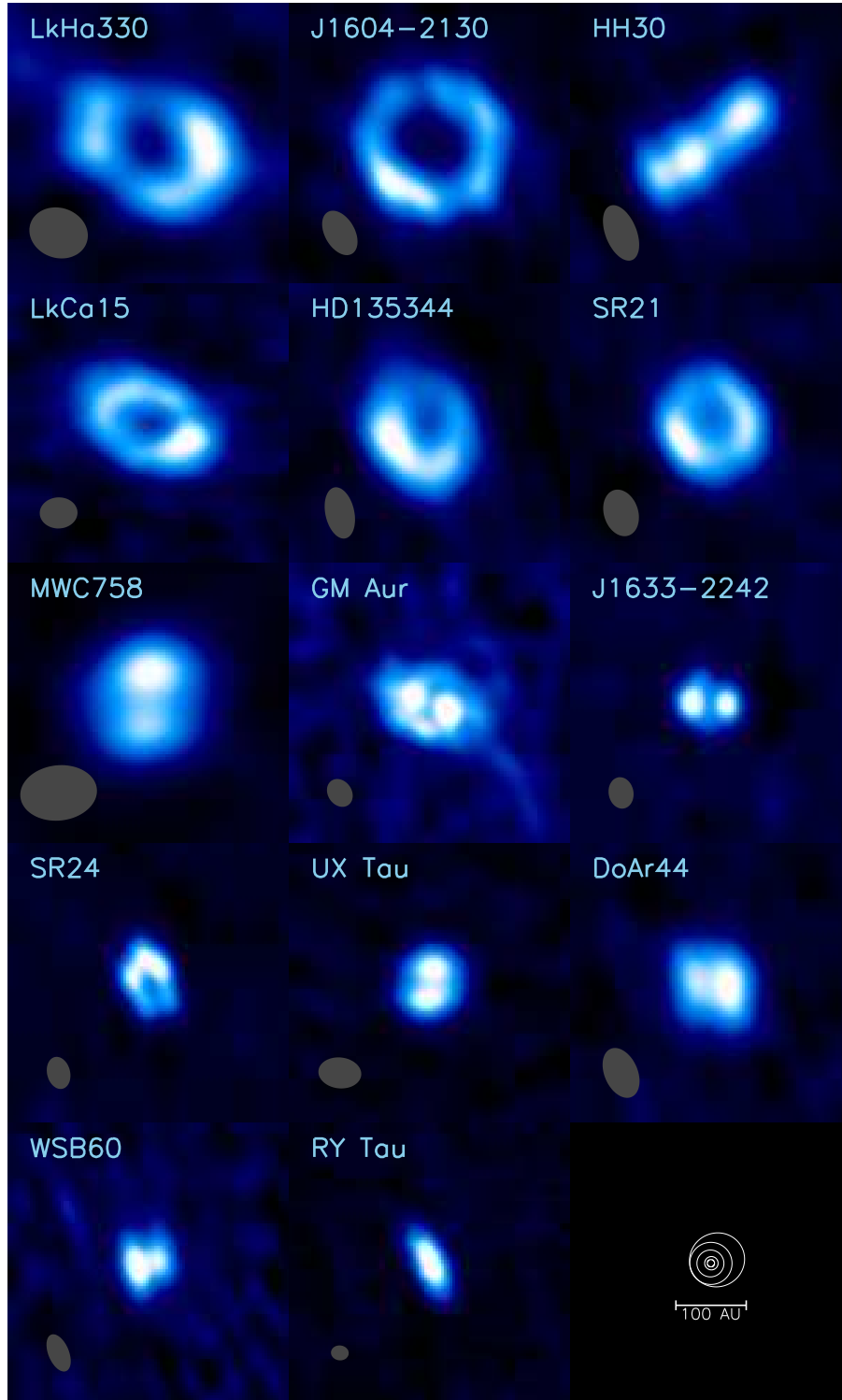


Figure 11: Montage of (sub-)millimeter images of protoplanetary disks with resolved inner holes. Each panel is 400 AU on a side, and the images are shown stretched over 99% of the range from minimum to maximum. The gray ellipse at the lower left of each panel shows the synthesized beam size, and ranges from $0''.15$ to $0''.8$. The orbits of the giant planets and Pluto in the Solar System are shown in the lower right panel for scale. The data are from a variety of published studies with the *SMA*, *Plateau de Bure*, and *CARMA* interferometers (Andrews et al. 2010b, Brown et al. 2009, Guilloteau et al. 2008, Hughes et al. 2009a, Isella, Carpenter & Sargent 2009, Piétu et al. 2006) as well as not yet published results.